Flow, water mass changes, and hydraulics in the Bosphorus

Michael C. Gregg
College of Ocean and Fishery Sciences, University of Washington, Seattle, Washington, USA
Applied Physics Laboratory, University of Washington, Seattle, Washington, USA

Emin Özsoy
Institute of Marine Sciences, Middle East Technical University, Erdemli, Turkey

Received 9 June 2000; revised 20 June 2001; accepted 3 July 2001; published 7 March 2002.

[1] Using average sections along the Bosphorus taken in September 1994 with a loosely tethered profiler and an acoustic Doppler current profiler, *Gregg et al.* [1999] found the exchange flow between the Sea of Marmara and the Black Sea to be quasi-steady but far from satisfying the hydraulic control conditions for two-layered flows. Here we examine synoptic sections and use images from an acoustic backscatter system to provide the first detailed look at the flow and water mass changes in the Bosphorus and to assess how well the flow satisfies the hydraulic assumptions. Thirty kilometers long, 28–100 m deep, and 0.75–3 km wide, the Bosphorus has bathymetry for more complex than that used in analytic or numerical models of exchange flows. The particulars affect dynamics in important ways. For instance, owing to changes in channel shape, the narrowest section, known as the contraction, is not also the minimum in cross-sectional area. Rather, it is a transition between the wider northern half and the narrower southern half of the strait, and some places south of the contraction have slightly smaller areas. Sharp bends occur throughout the strait and often produce flow separations as well as directing upper and lower flows to opposite sides of the channel. Never <28% of the water column, the interface thickens to 75% in the southern half of the strait as a result of intense mixing downstream of the contraction. As a consequence of the strong mixing and numerous flow separations, we conclude that the exchange flow may be at least partly controlled by friction instead of being a simple hydraulic flow. *INDEX TERMS:* 4568 Oceanography: Physical: Turbulence, diffusion, and mixing processes; 4223 Oceanography: General: Descriptive and regional oceanography; 4243 Oceanography: General: Marginal and semi-enclosed seas; 4219 Oceanography: General: Continental shelf processes; *KEYWORDS:* straits, hydraulic controls, mixing, turbulence, Bosphorus

1. Introduction

[2] Discovered long ago, the exchange flow through the Bosphorus inspired the first published fluid dynamics experiment [*Marsigli*, 1978]. The Bosphorus runs approximately north-south, connecting the Black Sea to the Sea of Marmara and ultimately to the Mediterranean (Figure 1). The exchange flow is characterized by brackish water flowing southward from the Black Sea and salty water flowing northward from the Sea of Marmara. The salinity contrast driving the baroclinic part of the flow is relatively steady, but the sea level difference forcing the barotropic component varies with the weather. Sometimes, northerly winds increase sea level at the Black Sea entrance so much that the barotropic flow cancels the baroclinic flow. In spite of this general understanding of the exchange flow, specifics remain uncertain, precluding realistic modeling or even definitions of the minimum set of parameters needed to predict the flow. Owing to the worsening ecology of the Black Sea [*Ünlüata et al.*, 1993] and to increasing ship traffic through the heart of Istanbul, the need for a much better understanding has become urgent.

[3] To obtain the first detailed look at the Bosphorus, in 1994 we took closely spaced sections with our loosely tethered Advanced Microstructure Profiler (AMP), which can be deployed even in urban settings (Figure 2), while monitoring the flow with two moorings and geodetically leveled tide gauges. To avoid major fluctuations in sea level difference, we worked during the weak winds of early September. *Gregg et al.* [1999] (hereinafter referred to as GOL) reported that the current meters revealed flow changes of ±30% in the lower layer and classified the flow as quasi-steady.

[4] GOL averaged density and along-channel velocity into 1 km bins along the thalweg and then applied the criteria for hydraulic control of inviscid two-layer flows to each bin. Observed average velocities were much too small to satisfy the criteria. The flow, however, was quasi-steady, demonstrating that it was in fact controlled, or limited, by friction and/or hydraulic constraints. Here we explore the details of the flow for clues about the processes at work.

[5] As a long, narrow, and shallow strait (Figure 1), the Bosphorus should be strongly affected by friction. This appears to be the case. Even when the forcing is most steady, the exchange flow appears to be complex and affected by local details. We seek to determine the structure and evolution of the northward and southward flows and whether there were signatures of strong mixing and hydraulic controls. As the first study of the particulars of the flow throughout the strait, we present enough detail to provide background for a following study using the microstructure data we collected in 1994 and to guide future observations that will be needed to understand better this complex system.

[6] After a brief review of hydraulics in section 2 we describe the instruments and observations in section 3. We take an overview of the measurements to look at the strait as a whole in section 4. Beginning with the bathymetry and channel shape, we then consider the barotropic and baroclinic forcing and follow with the evolution of the interface, transport, and θS relations. We then

0148-0227/02/2000JC000485

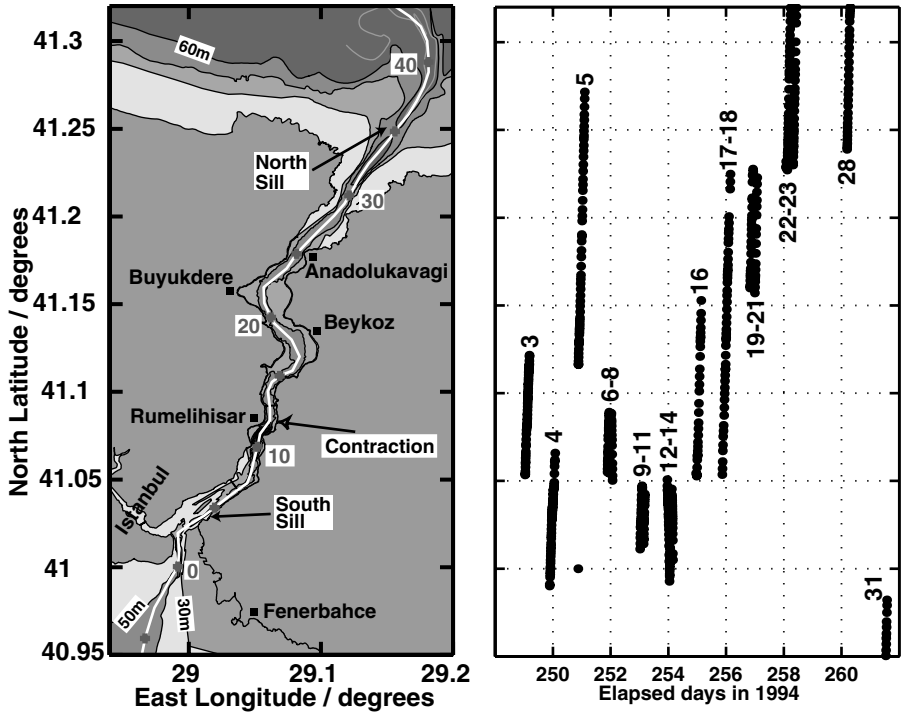

Figure 1. (left) Coastlines and bathymetry of the Bosphorus. The thalweg, shown by the white line, is marked at 5 km intervals from an origin at 41.004°N and 28.9916°E, just south of the Sea of Marmara entrance. (right) The latitudes of all AMP drops are plotted versus elapsed decimal days beginning with 0 for 1 January. Times are UTC, and day 249 was 7 September. The drops occurred in bursts that are numbered.

concentrate on the places of greatest interest in sections 5–7. We summarize in section 8, and discuss the significance of our findings in section 9.

[7] Although we find some situations where the flow seems to be hydraulically controlled, our thesis is that friction and the very irregular bathymetry play major roles in the Bosphorus. If we are correct, details matter and measurements at a few control points are not sufficient for a first-order understanding of the flow. We have not achieved that level of understanding, and more process-oriented observations will be needed. Consequently, we describe key locations in detail and point out the limitations of our measurements as well as what we believe they show about dynamics and mixing. In addition to being places where work is needed to understand the dynamics of this strait, some are also excellent sites to study specific processes of general interest.

2. Background

[8] Exchange flows occur where a basin (or reservoir) is connected through a constriction to another basin with denser fluid. The horizontal pressure gradient resulting from the density contrast (baroclinic forcing) drives the lighter fluid through the constriction as a surface flow above the denser fluid moving in the opposite direction. Sea levels often differ between the two basins, producing a horizontal pressure gradient (barotropic forcing) that tends to move fluid out of the higher basin. Barotropic forcing is constant with depth, depending only on the local surface slope, but baroclinic forcing increases downward in the constriction, owing to the cumulative effect of the lateral density contrast. When the basin with the lighter fluid is also higher, as in the Bosphorus, the two flows are separated by a no-flow surface along which the oppositely directed barotropic and baroclinic forcings balance each other, assuming that frictional stresses are negligible.

[9] Above and below the no-flow surface the net horizontal pressure gradient accelerates flows until further increases are limited by internal hydraulic controls and/or by frictional stresses. The theory of internal hydraulics is developed assuming that the flow is steady, inviscid, nonrotating, and hydrostatic. For this to be achieved, constrictions must vary gradually to avoid flow separations. To obtain tractable analytic solutions, most of the initial work considered two-layer flows and simple geometries, e.g., lateral contractions with vertical side walls and flat bottoms. For this case, *Armi and Farmer* [1986] found that the flow is hydraulically controlled where the composite Froude number G is unity, i.e., where

$$G^2 \equiv F_1^2 + F_2^2 \equiv \frac{u_1^2}{g'h_1} + \frac{u_2^2}{g'h_2} = 1, \tag{1}$$

where $g' \equiv g(\rho_2 - \rho_1)/\bar{\rho}$ is reduced gravity; u_1, h_1, and ρ_1 are the velocity, thickness, and density of the upper layer; and u_2, h_2, and ρ_2 characterize the lower layer. The flow is termed subcritical or supercritical where $1 < G^2 > 1$. *Lawrence* [1990] demonstrated an additional condition, namely, the flow must be stable to long internal waves. This occurs when the stability Froude number is <1:

$$F_\Delta \equiv \frac{|u_1| + |u_2|}{\sqrt{g'D}} < 1, \tag{2}$$

where $D = h_1 + h_2$ is the water depth.

[10] *Dalziel* [1991] demonstrated that the condition for critical flow can be restated as

$$G^2 \equiv 1 + \frac{C_1 C_2}{h_1 h_2}, \tag{3}$$

where C_1 and C_2 are the phase velocities of two mode-1 long internal waves, normalized by $\sqrt{g'D}/2$. At a control, where the

Figure 2. Launching an AMP in the southern Bosphorus, about 8 km from the Marmara entrance and looking toward the Asian side, which rises steeply behind a narrow beach. A probe guard was mounted on the bottom of the instrument to permit landing on the bottom. The thin blue tether transmitted data via a fiber-optic cable inside a Kevlar jacket for strength. The tether passed through a pulley mounted on the end of a fiberglass pole. The stiff, but flexible, pole damped sudden jerks on the line during recovery.

flow is critical and $G^2 = 1$, C_1 or C_2 must be zero. Where the flow is subcritical, $G^2 < 1$, C_1 and C_2 have opposite signs and can propagate in both directions. Where the flow is supercritical, $G^2 > 1$, C_1 and C_2 have the same sign, and both waves propagate away from the control into a basin. Consequently, changes within that basin cannot propagate back to affect the controls or the other basin.

[11] For simple geometries at least, there are usually two places where $G^2 = 1$. One control is set by the topography and occurs in the throat of a contraction or on the crest of a sill. The other, known as the virtual control, is upstream of the topographic control relative to the faster flow [*Armi and Farmer*, 1986; *Farmer and Armi*, 1986]. The flow is subcritical between the two controls and supercritical outside, until hydraulic jumps adjust the streams to conditions within the basins. When the opposing transports are equal, the two controls coalesce at the topographic control and the subcritical vanishes. Transports through a strait are greatest, i.e., the exchange is maximal, when flows are supercritical on both sides of the strait, even if the flow changes with time and is frictional [*Armi and Farmer*, 1987]. Only processes in the subcritical region between the controls affect the exchange flow. When the flow is supercritical on only one side of the strait, transports can never exceed those during maximal conditions and are usually smaller because they are affected by processes on the subcritical side.

[12] A number of studies have examined the effects of departures from the hydraulic assumptions and simple geometry. *Pratt et al.* [2000] evaluated hydraulic control within Bab al Mandab by solving the Taylor-Goldstein equation for the irregular cross-channel topography and observed velocity and density profiles. When they used monthly means, the flows were nearly always subcritical, i.e., $C_1 < u_{min} < u_{max} < C_2$, where u_{min} and u_{max} are the minimum and maximum velocities in the profile. The wave speeds, however, were not much smaller or much larger than the extrema. Consequently, using instantaneous profiles that included the tides produced critical and supercritical cases, implying that hydraulic control is intermittent. The authors note, however, that several tidal cycles are needed for a wave to traverse the sill and suggest that a more complete assessment of control would require demonstrating that long waves can cross the sill.

[13] *Pratt* [1986] and *Bormans and Garrett* [1989] analyzed the effects of interfacial friction and found that it did not fundamentally change the flow from the hydraulic solution. Bormans and Garrett, however, also considered friction at sloping side walls and found much larger effects. More recently, using an orthogonal curvilinear coordinate system to represent accurately flow through a contraction, *Winters and Seim* [2000] numerically investigated the effects of interfacial and bottom friction on exchange flows. Adding interfacial friction produced shear instabilities, which were resolved by the fine grid and produced large amounts of mixed water. The exchange remained symmetric about the throat, and on both sides the faster layer entrained the slower and carried the mixed water with it out of the contraction. Hydraulic controls were similar to the inviscid case, and the flow remained maximal. The positions of the controls, however, differed substantially, and the flows returned to subcritical short distances downstream, presumably because the model captured the internal hydraulic jumps. Although adding bottom friction did not increase average eddy viscosity in the domain, it greatly altered the dynamics and shifted

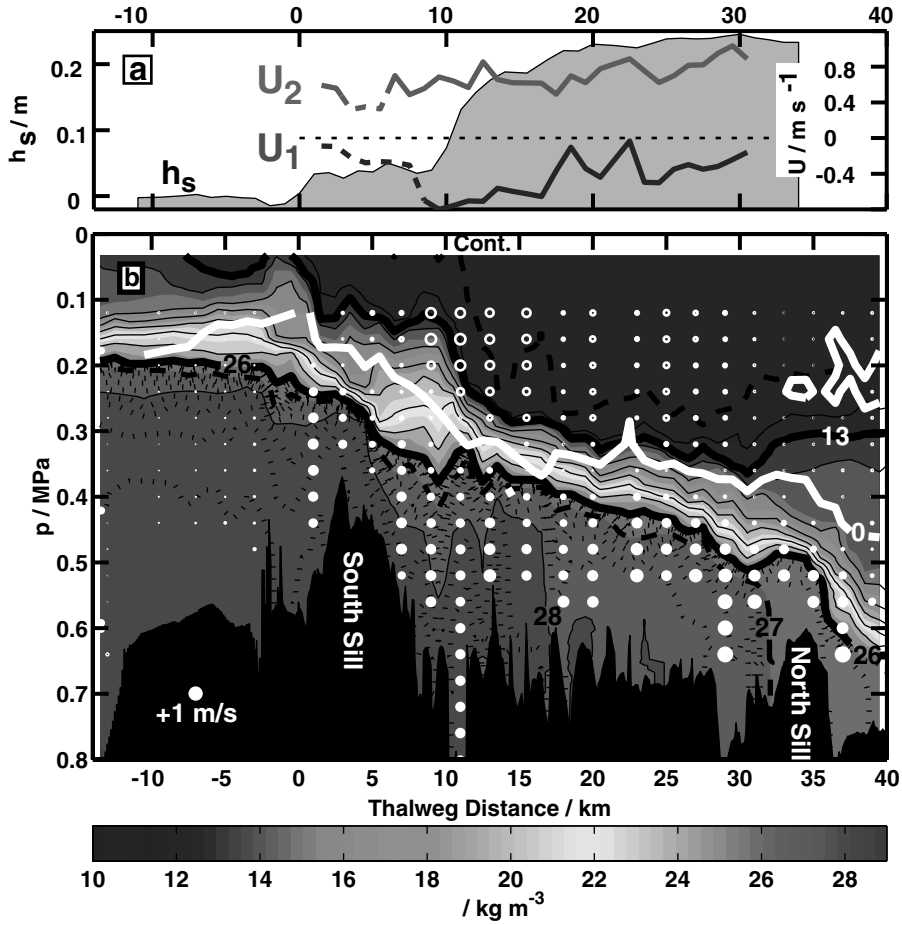

Figure 3. (a) Estimated sea surface height (shaded) and average along-channel velocities in the upper (blue) and lower (red) layers. Dashes show where we know the velocities are underestimates. Because the ADCP did not measure flows shallower than 0.12 MPa, U_1 seriously underestimates upper layer flow south of 8 km. (b) Contours of average potential density (black). Several isopycnals are labeled, and the color bar gives the full range. The two dark isopycnals, σ_θ = 13 and 26, bound the major stratification in the interface, and dotted lines in the lower layer show density intervals of 0.2 kg m^{-3}. Along-channel velocities, averaged in 2-km bins, are plotted as circles, which are solid where the velocity is positive. The thick white line is the zero isotach.

the exchange from maximal to submaximal. When the bottom boundary layer was an appreciable fraction of the lower layer, the drag decreased the composite Froude number so much that it was much less than one nearly everywhere. It rose to $G^2 = 1$ over such a short distance that the authors doubt that the control could be found in a field experiment. The exchange also became very asymmetric. The interface was flat on the light side of the contraction and rose steeply and thickened rapidly on the dense side as the light water accelerated and mixed. Most of the transport leaving the contraction toward the dense basin was in the interface.

[14] Using the same numerical code, *Hogg et al.* [2001a] found that changing the level of turbulence produced a continuous shift from flow satisfying the hydraulic assumptions to one dominated by viscosity. Their results are consistent with analytic solutions for both limits. Fluxes and volume fluxes depend on three dimensionless parameters: D/L, the aspect ratio; $Gr_T \equiv g'D^3/K_v^3$, the turbulent Grashof number; and $Pr_T \equiv K_v/K_\rho$, the turbulent Prandtl number, K_v and K_ρ are the eddy coefficients for momentum and mass. *Hogg et al.* [2001a] used $Pr_T = 1$, and the mass flux depended on $Gr_T(D/L)^2$. By comparing reported values of interface thickness with their calculations they estimated $Gr_T(D/L)^2 = 10^4$ for the Strait of Gibraltar and 5×10^{-3} for the Bosphorus. Calculated flows matched the hydraulic limit when $Gr_T(D/L)^2 \approx 10^7$ and the viscous-advective-diffusive limit when $Gr_T(D/L)^2 \approx 10^2$. Hence the Bosphorus is nearer the latter, and Gibraltar is close to the former.

[15] *Hogg et al.* [2001b] considered hydraulic control in continuously stratified fluids by studying the propagation of linear internal waves in the flow fields of their previous study. One approach was to track waves generated mechanically where the stratification was greatest and then evolving with linear dynamics. The other approach used eigenvalue solutions from sixth-order stability theory of parallel shear flows to interpret the evolution of the test waves. They identified two types of mode-1 solutions capable of transmitting information about baroclinic changes in the basins along the entire channel: density modes, appearing only when viscosity is not zero and having eigenfunction maxima centered on the peak stratification, and vorticity modes, with maxima close above and below the stratification peak. Sites where mode-1 density waves have a phase velocity of zero seem analogous to topographic controls of hydraulic theory and were found at the contraction throat. Sites where mode-1 density modes have zero crossings seem analogous to virtual controls of hydraulic theory, shifting upstream with increasing barotropic flow and carrying information out from the zero crossing. Vorticity modes evolve gradually along the channel as their maxima shift vertically and cross the stratification maximum. These transition zones

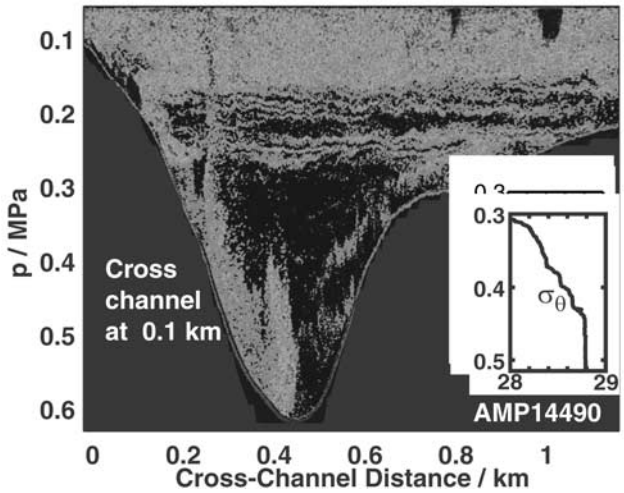

Figure 4. Acoustic backscatter and stratification across the Marmara entrance channel at 0.1 km on the thalweg. Pixels in the image have been colored to show the intensity of the backscatter, dark red for intense through yellow and blue to black for no return. The insert shows a density profile taken nearby several days later. The outfall of Istanbul's main sewer extends down the west side of the channel and ends in the middle. Its rising plume was trapped by the strong stratification above the homogeneous bottom boundary layer.

appear to be sites of controls present in viscous flows having continuous stratification. Hence there are no analogs in inviscid two-layer flows.

[16] Applying *Hogg et al.* [2001b] to our data is beyond the scope of this paper. Instead, we limit our discussions of hydraulics to evaluating the hydraulic criterion (1) with instantaneous sections rather than the cruise-average sections applied by GOL. Doing so appears to resolve some issues but raises other questions that will be addressed in the future after we have compared our turbulence measurements with inferences of mixing in this paper based on θS changes and large-scale signatures.

3. Observations and Instruments

[17] Before beginning shipboard profiling we set moorings at 8.0 and 12.0 km along the thalweg or deepest path. Distances are positive northward from an origin at 41.004°N, 28.9916°E in the Marmara entrance (Figure 1). Each mooring had two Anderra current meters with temperature and conductivity recorders. The lower meters were 8 m above the bottom, and to avoid supertankers the upper meters were set 22 m below the surface (0.22 MPa). Our colleague, M. Latif, installed geodetically leveled pressure gauges at Anadolukavağı and Fenerbahçe.

[18] We worked from the R/V *Bilim*, operated by the Middle East Technical University. To avoid the intense shipping and ferry traffic in the restricted southern half of the strait, we operated at night, generally between 2300 and 0700 LT or 2000–0400 UTC. All times are in yeardays, with yearday 0 beginning at 0000 UTC on 1 January. Observations in the strait began on 7 September (yearday 249) and ended on 19 September (yearday 261).

[19] The *Bilim* carried a narrowband 150-kHz acoustic Doppler current profiler (ADCP). Its shallowest bin was at 0.1 MPa (10 m); it was usually operated with 4-m pulses and bins. The unit kept good bottom tracking, which was checked afterward against headings from a fluxgate compass we had installed and courses recorded using the ship's Global Positioning System receiver. We averaged the raw data in 5-min blocks for scientific analysis.

[20] The AMP provided the primary measurements. It was operated as before [*Seim and Gregg*, 1994], but this time each profiler also measured temperature with 20-bit resolution and had an 89-kHz acoustic altimeter accurate to 10 mm. Temperature and salinity profiles appeared free of surface transients below 0.03 MPa (3 m). Owing to the traffic lanes and swift currents, we made all AMP runs, termed bursts, along the channel (Figure 1b) with the *Bilim* passing over the bottom at 1–2 m s^{-1}.

[21] A 200-kHz BioSonics acoustics backscatter system yielded excellent images of mixing structures. *Seim et al.* [1995] demonstrated that acoustic backscatter from turbulence can exceed returns from biology, and *Seim* [1999] used some of our data from the Bosphorus to show that salinity microstructure can increase returns an additional factor of 10 when salinity controls the stratification. The backscatter cross section is proportional to a weighted sum of the temperature and salinity spectra at the scattering scales. Those spectra, in turn, depend on the turbulent dissipation rate and the magnitude of the gradients where the mixing occurs. Hence strong turbulence in a weakly stratified layer will not produce a strong return, but moderate turbulence in strong gradients may. Nearly all returns in the strait appeared to come from mixing or at least from specular reflection from density surfaces, primarily in the interface. Consequently, in addition to using backscatter images to reveal mixing structures, we also interpret variations in their magnitude as rough indicators of mixing intensity. Features with apparent horizontal length scales L in the images have a true wavelength of $\lambda_x = L(1 - u/u_{\text{ship}})$.

4. Overview of the Exchange Flow

4.1. Bathymetry and Bends

[22] Thirty kilometers long, 28–100 m deep, and 0.75–3.0 km wide, the Bosphorous has an average depth of 64 m and an along-channel aspect ratio of $D/L = 0.0021$ (Figures 1 and 3b). A typical cross-channel aspect ratio is $D/W = 0.06$. We reference positions to the southern entrance, where a small canyon leads dense water from the Sea of Marmara across the narrow shelf to South Sill (Figure 4).

[23] Using detailed seismic profiles, *Gökacsan et al.* [1997] argue that faulting largely controlled the evolution of the Bosphorous. They outline the sequence as beginning with two streams flowing in opposite directions from near Anadolukavağı (Figure 1), where uplifting produced a local high in the basement rock. One stream flowed north, toward the Black Sea, and the other flowed south, toward the Sea of Marmara. Block faulting then formed a basin, which the stream flowing south filled to form a lake between Beykoz and Büyükdere. Intense faulting during the Pleistocene formed grabens and offset them laterally, so that the stream following the grabens followed a convoluted path in filling the depressions to form a lagoon. Rising sea level eventually flooded the channels and connected the Black Sea to the Sea of Marmara. Many of the faults remain active, and the very rough bottom plus the sequence of grabens and lateral offsets in the southern two thirds of the strait strongly affects the exchange flow.

[24] South Sill (2–6 km) is the shallowest part of the strait. The deepest part, which we term the hole, is at 9.5–11 km. *Gökacsan et al.* [1997] attribute it to a "pull apart" basin formed by faulting. The hole ends at the narrowest section, known as the contraction (11–14 km). North of the contraction, the bottom is rough throughout. A steep-sided trough (29–31 km) separates the strait from the pre-Bosphorus channel, through which the dense water flows onto the Black Sea shelf. Cut by the original northward stream, the morphology of this part of the system is primarily fluvial rather than tectonic. The floor of the channel rises to North Sill at 33–36 km before descending and curving west. On the basis of a two-dimensional numerical model, *Oğuz et al.* [1990] identify

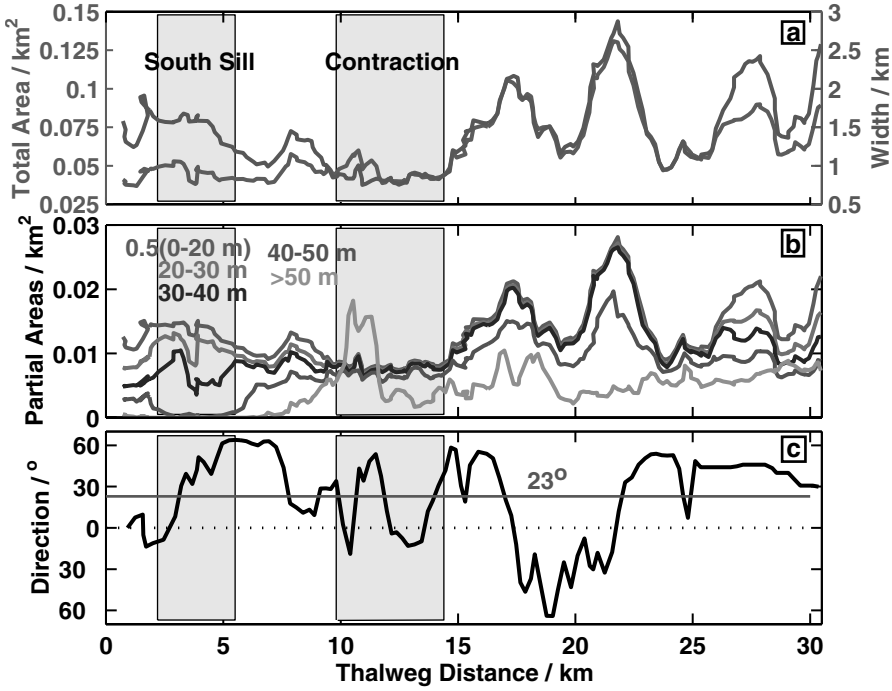

Figure 5. (a) Width and total cross-sectional area. The contraction is a minimum in width but not in area. (b) Partial cross-sectional areas. The cross-sectional areas between successive isobaths demonstrate how the depth-dependent narrowing varies along the strait. The hole at 11 km produces the large spike in areas from depths below 50 m. (c) Channel direction, in 0.25-km increments along the centerline. The direction from south to north varies between, ±64° from north. The average is 23°.

South Sill, the contraction, and North Sill as sites where the exchange flow is controlled hydraulically.

[25] The northern half of the strait is both wider and more variable in width than the southern half. To determine how well cross-sectional area follows the variations in width, we digitized coastlines and bathymetry from the chart İSTANBUL BOĞAZI [*International Oceanographic Center*, 1985] and supplemented the soundings with our digitized BioSonics records. Figure 5a compares width and area, and Figure 5b shows the areas of successive 20-m depth intervals. Area closely follows width between 12 and 26 km but not elsewhere.

[26] Of particular importance to the dynamics are the following.

1. Both width and total area have local minima and maxima that repeatedly accelerate and decelerate the flow.

2. Cross-sectional area in the southern half of the strait is notably smaller than in the northern half. The contraction is the transition between the two regimes.

3. Although the contraction is the narrowest part of the strait, it is not also a minimum in total cross-sectional area. In fact, its area is slightly larger than some places farther south, at least to the accuracy of these data. Specifically, the average area in the contraction is 0.046 km^2, compared to 0.037 km^2 at 1.3 km and 0.038 km^2 at 3.8 km.

4. The contraction, however, does have the least area shallower than 20 m, the maximum depth of the upper layer in the southern half of the strait. Consequently, the upper and lower layers may not have hydraulic controls at the same places.

Thus, rather than being a choke, the contraction is more of a transition in cross-sectional area.

[27] In addition to its irregular depth and width, the channel also turns sharply about its average orientation of 23° true from the southern entrance (Figure 5c). Immediately north of the contraction, the strait twists through 128° in a few kilometers. Within the contraction the channel turns 60° and then bends back by nearly the same amount immediately to the south. Over South Sill the direction changes about 90°. Bends of this magnitude can be expected to affect the dynamics of the flow, especially in view of the matching changes in area. Adverse along-channel pressure gradients should be common close to sharp expansions [*Signell and Geyer*, 1991], and in fact, we often found flow separations at these places. Pilot charts for the Bosphorus show separated flow downstream of nearly every bend and expansion, a condition recorded since Jason and his Argonauts "set off under sail through the eddying Bosporos" [*Apollonius of Rhodes*, 1993]. We passed through several flow separations and, indeed, found very weak currents and sometimes reversals in direction. They were most obvious in the shallow flow, but some also occurred in the lower layer.

4.2. Forcing

[28] As described by GOL, in response to atmospheric pressure changes, the leveled tide gauges showed a range in sea level difference of $\Delta z_0 = 0.2-0.45$ m. The average was 0.32 m, and tidal amplitudes were only 10 mm. By neglecting turbulent stresses, GOL used their average subsurface density field to estimate the surface heights required to produce no horizontal pressure gradients on the surface of no mean flow observed with their ADCP. The steepest surface slope was across the contraction (Figure 3a) and corresponded to a slope of 0.0034° over 1 km.

[29] Baroclinic forcing resulted from the large contrast between dense Marmara and light Black Sea waters. Both inflows were stratified, as seen in the profiles at 0.1 and 32.4 km (Figure 6a). The Black Sea inflow included densities with $10.5 \leq \sigma_\theta \leq 14.6$ and averaged 12.1 kg m^{-3}. The bottom of the Black Sea inflow contained the upper part of the Cold Intermediate Water (CIW), which was strongly stratified by temperature. The bottom of this inflow contained a thin region of mixed water that it entrained and carried back into the strait. The Marmara inflow came from the base of the pycnocline and spanned densities with $21 \leq \sigma_\theta \leq 28.8$. It averaged 27.7 kg m^{-3} and was stratified by salinity. The upper

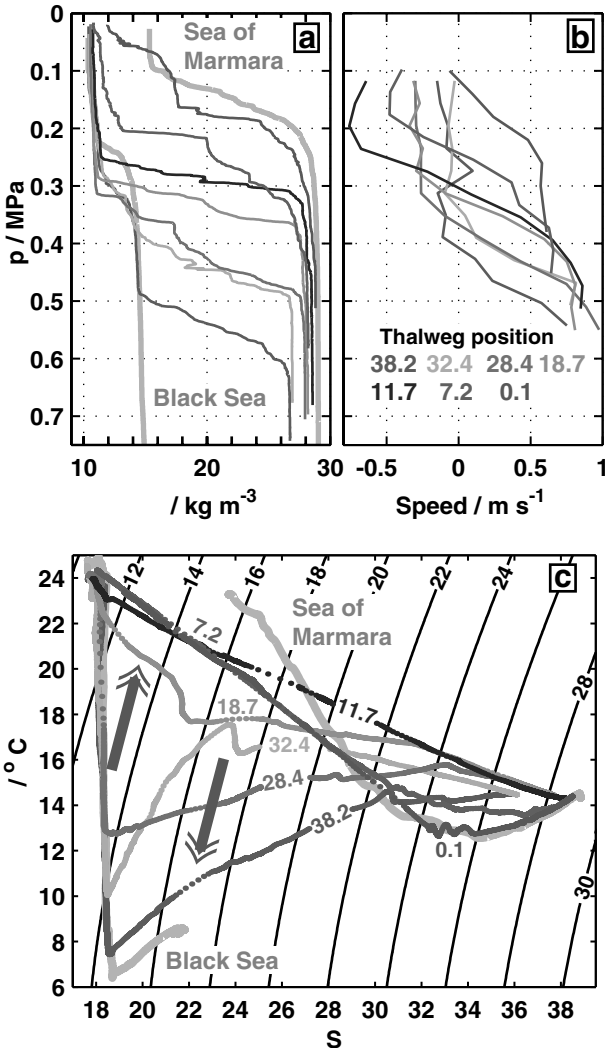

Figure 6. (a) Representative σ_θ profiles along the strait compared with ones in gray taken in the Black Sea and Sea of Marmara away from the direct influence of the Bosphorus. (b) Matching speed profiles with northward flow positive and southward flow negative. (c) The θS relations for the profiles in Figure 6a. Note that only for $\sigma_\theta > 21$ does the water at 0.1 km follow the Marmara θS relation. The Bosphorus profiles and their burst numbers are 38.2 (AMP14885, burst 22), 32.4 (AMP14870, burst 22), 28.4 (AMP14821, burst 17), 18.7 (AMP148000, burst 17), 11.7 (AMP14785, burst 17), 7.2 (AMP14525, burst 4), and 0.1 km (AMP14490, burts 4). The reference profiles (gray) are AMP14961 (burst 27) in the Black Sea and AMP14746 (burst 15) in the Sea of Marmara.

part of the Marmara inflow included entrained mixed water, and the lower part contained a temperature minimum.

[30] Synoptic weather systems lasting 3–5 days produced the fastest significant changes in sea level. Traveling the 30-km strait at a speed of $c_1 = 1.2–1.7$ m s^{-1}, internal responses would transit a quiescent strait in only 5–7 hours, or 7/120 = 1/17 of the forcing period. This is close to the ratio of 1/30 that *Helfrich* [1995] considers necessary for the application of classical hydraulic theory.

[31] The internal radius of deformation is $R_c = (g'h_1)^{1/2}/f$, where f is the Coriolis frequency. For the Bosphoros, R_c = 17–29 km, greatly exceeding the 3 km maximum width. Consequently, the Earth's rotation is unlikely to affect the flow significantly.

4.3. The Interface

[32] Density contours (Figure 3b) and representative profiles along the strait (Figure 6a) reveal well-mixed surface and bottom layers separated by strongly stratified interfaces. Transitions from weak to strong stratification were gradual in some profiles and abrupt in others, frustrating simple definitions of the interface. Because σ_θ = 13 and 26 were everywhere within the interface, we highlighted them in Figure 3b to mark the most conservative boundaries. To obtain more accurate boundaries, we took an approach similar to locating the bottoms of surface mixed layers: p_1 and p_2 were defined as the pressures where σ_θ differed by 0.5 kg m^{-3} from the surface and bottom densities. These are compared with the pressure of no mean flow p_{nf} (Figure 7a) and were used to compute thicknesses of the upper, h_1, and lower, h_2, homogeneous layers. The separation between p_1 and p_2 is the interface thickness h_i. It averaged 29 m and varied between 17 and 49 m, or 28 and 75% of the depth (Table 1).

[33] Simply from the thickness of the interface, it is clear that conditions in the Bosphorus were not a simple two-layer exchange. At the Black Sea entrance, half of the dense outflow and 20% of the light inflow were in the interface. Figure 7a shows that the interface was thinnest, 17 m, at 19.5 km and thickest, 49 m, at 9.5 km. Most of the thickening occured in the southward flow, i.e., where $p < p_{nf}$.

4.4. Transports and Transit Times

[34] To estimate southward and northward transports, Q_S and Q_N, we assumed that the velocity was constant from the shallowest ADCP bin to the surface. We also assumed that the deepest speeds not contaminated by ADCP side lobes were constant from the deepest measurement to 5 m above the bottom and then linearly decreased them to zero. Multiplying profiles of mean speed and cross-sectional area in each 1-km bin along the thalweg gave the transports (Figure 7d).

[35] South of 3 km and north of 26 km, Q_N has little scatter, which we attribute to the relatively straight bathymetry. These values are close to the mean and median values of Q_N: 10.7×10^3 and 11.0×10^3 m^3 s^{-1}. The scatter in Q_N between 3 and 24 km seems to result from inadequate sampling near bends, where the flow was not uniform across the channel, and over the sill, where much of the deep flow was too close to the bottom to be detected with the ADCP. Because a large part of the upper, or southward, flow was deflected onto shallow banks downstream of bends, the Q_S estimates have more scatter than those of Q_N. The largest departures from the mean occurred between 15 and 20 km, where the bends are largest (Figure 5c) and the shoals are wide (Figure 1). In addition, the southward flow shoaled rapidly south of 8 km, producing a large underestimate. Considering only estimates north of 8 km, the mean and median of Q_S are -16.3×10^3 and -15.6×10^3 m^3 s^{-1}.

[36] For comparison, *Özsoy and Ünlüata* [1997] estimated long-term means as $\overline{Q_N} \approx 10.0 \times 10^3$ m^3 s^{-1} and $\overline{Q_S} \approx -20.0 \times 10^3$ m^3 s^{-1}. Our values are about 10% larger for $\overline{Q_N}$ and 25% smaller for $\overline{Q_S}$. The differences between our transports and the long-term averages are less than the known variability of the flow and hence consistent with previous observations. The mean and median net transports, i.e., $Q_S + Q_N$, are -5.6×10^3 and -4.6×10^3 m^3 s^{-1}. In terms of the flux ratios specified in models of exchange flows, these give $q_r \equiv |Q_S|/|Q_N| = 1.52$ and 1.42, indicating moderate barotropic flow compared to the long-term mean of $q_r = 2$ [*Özsoy and Ünlüata*, 1997].

[37] Figure 7d also reveals how the transport was distributed between the homogeneous layers (dashed lines) and the interface (dotted lines). At the Marmara entrance, nearly all of the northward transport was in the interface. The ratio began varying north of 10 km and finally stabilized at about 50/50 past 15 km, the north end of the contraction and past the hole. This implies an entrainment of part of the northward interface into the bottom layer in this section.

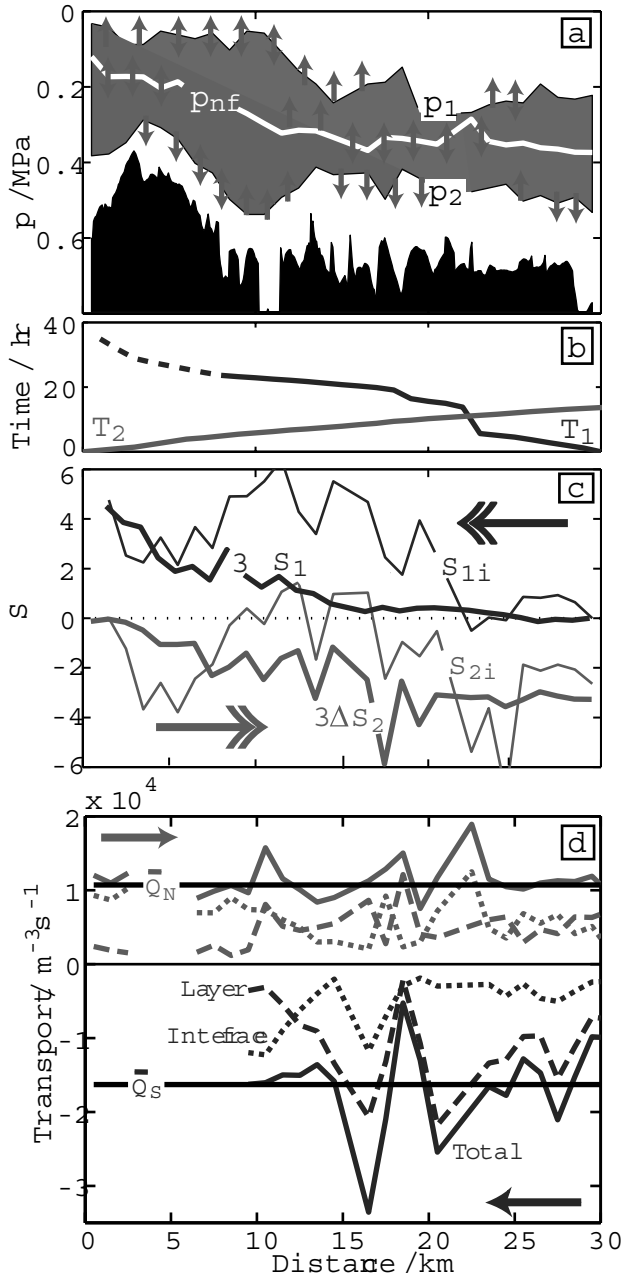

Figure 7. (a) Interface boundaries, defined in Table 1, and salinity fluxes. Arrows show salinity fluxes inferred from the salinity changes in Figure 7c. Single arrowheads are placed where the layer pointed to was changing but the other layer was not, for example, lower homogenous layer was becoming fresher while the salinity of lower interface was not becoming more saline. Double arrowheads mark complimentary changes across boundaries, for example, the lower interface was becoming more saline while the lower homogenous layer became fresher. (b) Cumulative transit times for the layers. T_1 is dashed where the estimates are unreliable. (c) Salinity changes within the strait. Changes in the layers, ΔS_1 and ΔS_2, were multiplied by 3 to show them on the same scale as the changes in the interfaces, ΔS_{1i} and ΔS_{2i}. (d) Northward and southward transports for each 1-km bin along the thalweg using the average northward and southward speed profiles and the cross-sectional area averaged for the bin. Solid black lines are the mean values. Owing to the severe underestimate of southward transport south of 8 km and of northward transports over South Sill, those values are omitted.

[38] The composition of the southward flow also changed, with the fraction carried in the interface increasing. Black Sea water entered with most of the flow in the surface homogeneous layer. It exited with most of the transport in the interface. Omitting the oscillations between 20 and 15 km as being unreliable, most of the transport was still in the surface layer as the flow entered the contraction south of 15 km. Through the contraction to 9 km, i.e., as far as the transports seem reliable, the interface entrained the surface layer and rapidly dominated the southward transport.

[39] On the basis of our 1 km average speeds the lower layer was significantly faster than the upper in most of the strait. It transited the strait in 16 hours with $\overline{u_2} \approx 0.52$ m s^{-1}, compared to the 27 hours taken by the upper layer to reach 8 km at $\overline{u_1} = -0.23$ m s^{-1}. The pronounced slowing near 22 km, indicated by the steep slope in T_1, occurred where the width and area are greatest (Figure 5a), but owing to the bends, it is likely that we missed some of the flow and that T_1 is overestimated here. Even if u_1 averaged 1–1.5 m s^{-1} south of 8 km, the southward flow would have required several more hours to reach the southern exit from 8 km. If this compensates for the overestimate of T_1 near 23 km, the southward transit takes about 1.7 times longer than the northward transit.

[40] Neglecting friction and using Bernoulli's relation to estimate an upper bound on the surface speed, we find at the south end, $u_0(0.5\text{ km}) = [2g\Delta z_0 + u_0^2(29.5\text{ km})]^{1/2}$, where Δz_0 is the sea level difference across the strait measured by leveled tide gauges (GOL). For $\Delta z_0 = 0.32$ m and $u_0(29.5\text{ km}) = 0.2$ m s^{-1}, $u_0(0.5\text{ km}) = 2.5$ m s^{-1}. On the basis of ship drift we estimate maximum surface speeds of no more than 1.5 m s^{-1}, suggesting that friction and/or form drag were important.

4.5. Net Density and θ*S* Changes

[41] In addition to large density differences, the inflows carried strongly contrasting θ*S* structures into the strait. These differences and how they changed during their transits are summarized in Table 2 using average properties at the southern, 0.5 km, and northern, 29.5 km, entrances. The total southward flow, $p < p_{nf}$, entered with $\sigma_\theta = 11.2$ and exited with $\sigma_\theta = 14.2$, an increase of 3 kg m^{-3}. This resulted from $\Delta\theta = -0.5$°C and $\Delta S = +3.6$. By comparison the change in the total northward flow, $p > p_{nf}$, was modest, $\overline{\sigma_\theta} = 26.5 - 25.8$, a decrease of 0.7 kg m^{-3} resulting from $\Delta\theta = +0.1$°C and $\Delta S = -0.9$. Passing through the strait reduced the density contrast from $26.5 - 11.3 = 15.3$ kg m^{-3} between inflows to $25.8 - 14.2 = 11.6$ kg m^{-3} between outflows. This reduction was 24% of the initial contrast, implying a substantial amount of mixing and a net entrainment into the southward flow.

[42] The bottom homogeneous layer thickened from 21.5 to 30.0 m, while the total northward flow thinned from 58.0 to 46.0 m. The salinity of the lower layer decreased by 1.4, but this produced only a slightly larger reduction in density, −0.8 kg m^{-3}, compared to −0.7 kg m^{-3} for the entire northward flow. The upper layer salinity increased by 1.4, but it also cooled 0.8°C to produce a density increase of 1.3 kg m^{-3}, less than half the increase of the full southward flow. The larger changes in the southward flow compared to the northward flow indicate that it entrained proportionately more than the northward flow.

[43] To examine the structure of these changes, Figure 8 compares two-dimensional θ*S* histograms at the southern and northern ends of the Bosphorus. Histogram heights are in increments of 0.5 m, and the bins are $d\theta = 0.5$°C and $dS = 0.5$. Bins in the southward inflow are colored green: dark green for those in the 22.5-m-thick surface mixed layer and light green for those in the 15-m-thick pycnocline. All of these samples fell on the temperature-stratified Black Sea θ*S* relation, except for the bottom 2 m of the inflow. The northward inflow is colored red: dark red for the bottom boundary layer (21.1 m thick) and light red for the halocline (36.5 m thick). Most samples fell on the salt-stratified Marmara Sea θ*S* relation.

Table 1. Definitions of the Interface and Its Characteristics

Characteristic	Definition
p_{13}, p_{26}	pressures of σ_θ = 13 and 26 kg m^{-3}, which are always in the interface
p_1, p_2	pressures where σ_θ differs by 0.5 kg m^{-3} from surface and bottom values
h_1, h_2	thicknesses of upper and lower homogenous layers, based on p_1 and p_2
p_{nf}	pressure of zero mean isotach
h_i	interface thickness, $100(p_2 - p_1)$
h_{i1}	thickness of southward flowing portion interface, $100(p_{nf} - p_1)$
h_{i2}	thickness of northward flowing portion interface, $100(p_2 - p_{nf})$

[44] The southward outflow is colored blue: dark blue for the shallowest sample, which we assumed also represented the 3 m above it, and light blue for the 19.5-m-thick pycnoline. The northward outflow is colored brown: dark brown for the 30 m in the bottom boundary layer and light brown for the 28 m in the halocline. Both outflow relations differed markedly from their inflows and fell on straight mixing lines (thick black) that included several meters of the inflow above them. Specifically, at the northern end the bottom 2 m of the inflow (light green) was on the same mixing line as the outflow (brown); and at the southern end the upper 6.5 m of inflow (light red) was on the same mixing line as the outflow (blue). This demonstrates that these waters had been mixed in the strait and then were entrained into the opposite inflows.

[45] In summary, the northward flow was transformed from a homogenous bottom layer (21.1 m thick) and a halocline (36.5 m) containing a temperature minimum to a slightly less salty homogenous bottom layer (30 m) and a nearly isothermal halocline (16 m). The surface mixed layer (22.5 m) and thermocline (15 m) in the southward flow were compressed into a thin surface layer ($\leq$3 m) overlaying a pycnocline (9 m) stratified by salt and temperature. Salinity of the homogenous surface layer increased as much as the bottom layer decreased. The largest change was the increase in salinity of the southward flowing interface.

4.6. Where Mixing Occurred

[46] Figure 7c displays salinity changes in the homogenous layers (thick lines) and upper and lower portions of the interface (thin lines), i.e., using a four-layer decomposition of the flow. Because changes in the layers were considerably smaller than those in the interface, they are multiplied by 3 to use the same scale. Changes for the northward flow, ΔS_2 and ΔS_{2i}, are relative to average salinities at 0.5 km: S_2 = 38.37 and S_{2i} = 35.46. Southward changes were computed relative to averages at 30.5 km: S_1 = 17.80 and S_{1i} = 18.64. We cannot determine whether the short-length fluctuations resulted from cross-strait variability or temporal changes and concentrate on the more gradual trends. In some places the salinity changes imply entrainment of fluid into one layer without affecting the host layer. These are indicated by arrows with single heads in Figure 7a. Other places, however, experienced opposite changes across a boundary, implying two-way salt exchanges. These are marked with double-headed arrows.

[47] Four bursts of entrainment produced most of the freshening in the homogenous lower layer. Crossing South and North Sills generated two of the bursts, and rebounding from the two holes caused the other two. Isopycnals ending in the bottom mark these in Figure 3b, and the first three bursts are responsible for decreases of ΔS_2 in Figure 7c. The first burst began near the crest of South Sill and continued on the sill's gentle northern slope. The second was just north of the hole and in the large bends. Initially, the freshening of the lower layer was not accompanied by an increase in salinity of the lower interface, implying that turbulence in the lower layer generated downstream of the sill crest entrained some of the interface, but the remaining northward interface was unaffected. From 5 to 8 km, however, the lower interface became more saline while the bottom layer continued freshening. This indicates compensating fluxes, possibly by strong turbulent diffusion. North of 8 km, freshening of the bottom layer stopped, but the northward interface continued to become more saline, suggesting that it was entraining the bottom layer. The second freshening of the bottom layer was not accompanied by increasing salinity in the northward flow above it, indicating renewed downward entrainment in the section where we previously found a shift in the northward transports carried in the interface and bottom layer (section 4.4). After the northward flow left the strait it freshened again just north of the hole at 30 km, as is evident in the vertical isopycnals (Figure 3b).

[48] The homogenous surface layer was unchanged for the first few kilometers. Then from 28 to 21 km it gradually became more saline. Salinity in the southward interface initially decreased but then increased as mixing within the southward flow was overwhelmed by mixing between northward and southward flows. At 17 km, just north of the contraction, the surface layer began a more rapid increase in salinity that continued at roughly the same rate to the southern entrance. This coincided with the steady increase of interface transport at

Table 2. Average Properties and the Inflows and Outflows at 0.5 and 29.5 km and the Changes Between Them, Δ[a]

	Southward				Northward			
	h, m	S	θ, °C	σ_θ, kg m^{-3}	h, m	S	θ, °C	σ_θ, kg m^{-3}
				Total				
In	37.5	18.0	22.3	11.2	58.0	35.6	14.7	26.5
Out	12.0	21.6	21.8	14.2	46.0	34.7	14.8	25.8
Δ	−25.5	+3.6	−0.5	+3.0	−12.0	−0.9	+0.1	−0.7
				Homogenous Layers				
In	22.5	17.8	24.1	10.6	21.5	38.4	14.3	28.8
Out	$\leq$ 3	19.2	23.3	11.9	30.0	37.0	14.4	27.6
Δ	$\leq$ − 19.5	+1.4	−0.8	+1.3	+8.5	−1.4	+0.1	−0.8

[a] The upper half of the table, labeled Total, contains changes in the total southward and northward flows. That is, the changes are of a two-layer decomposition based on velocity and include water in the interface. The lower half of the table, labeled Layers, considers only changes in the upper and lower homogenous layers, based on density.

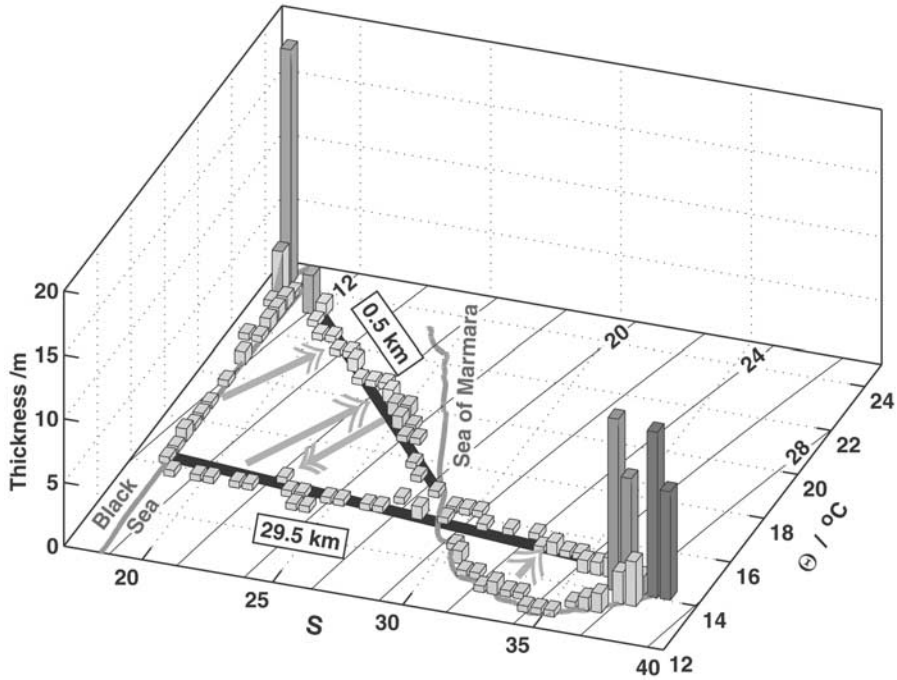

Figure 8. Histogram θS relations at the Marmara (0.5 km) and Black Sea (29.5 km) entrances. Southward flowing water at 29.5 km is plotted green when entering from the Black Sea and blue when exiting at 0.5 km to the Marmara. Northward flowing water is red when entering at 0.5 km from the Marmara and brown when exiting at 29.5 km to the Black Sea. In all cases, water in the upper and lower layers is dark, and that in the interface is light. The histogram bins have $d\theta = 0.5°C$ and $dS = 0.5$, and the gray lines show profiles taken well away from the Bosphorus. Thick black lines show mixing lines linking in and outflows.

the expense of the surface layer indicates rapid entrainment of the surface water by the interface. The surface layer, however, was also being modified, but as it was simultaneously thinning, this required decreased mixing with the more saline interface. There were small reversals in ΔS_1, but cross-strait variability cannot be distinguished from temporal changes.

[49] By far the largest changes took place in the upper and lower parts of the interface. These changes were not always monotonic, but they tended to track each other. For instance, during the transit from 13 to 23 km, $S_{2i} \approx -7$, while in the opposite direction, $S_{1i} \approx +6$. This could only result from mixing between the oppositely directed upper and lower parts of the interface. Similar changes also occurred between the Marmara entrance and the crest of South Sill. The other large changes in the interfacial layers took place between about 6 and 12 km but had the opposite sense, i.e., ΔS_{2i} increased while ΔS_{1i} decreased. In both cases there was net entrainment within the northward and southward flows from their homogenous to their stratified layers. In the next three sections we examine details of the flows where hydraulic controls have been identified in previous studies and where we found major mixing.

5. Flow Over South Sill

[50] Owing to the importance of South Sill as the shallowest part of the strait, we studied it intensively, taking 7 AMP bursts along the channel at different across-channel positions. The tracks and drop positions of four of these bursts are included in Figure 9.

5.1. Bathymetry

[51] Just as all unhappy families are unhappy in their own way [*Tolstoy*, 2000], so are all sills complex in unique ways. The

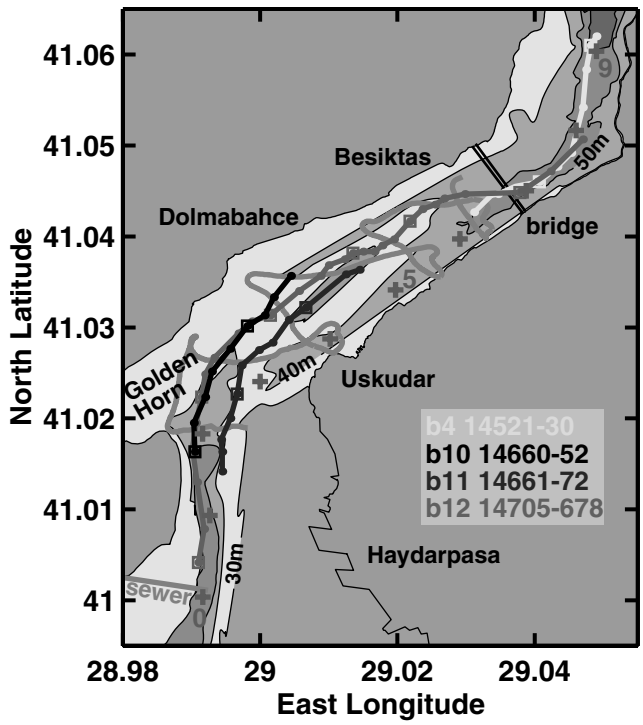

Figure 9. Bathymetry and some of our ship tracks in the southern third of the strait. Red crosses mark the thalweg at 1-km intervals. The gray ship track shows the runs used to fill in gaps in the bathymetry. The colored ship tracks show AMP bursts used in the text. Circles mark each AMP drop, and squares designate drop numbers that are multiples of 5.

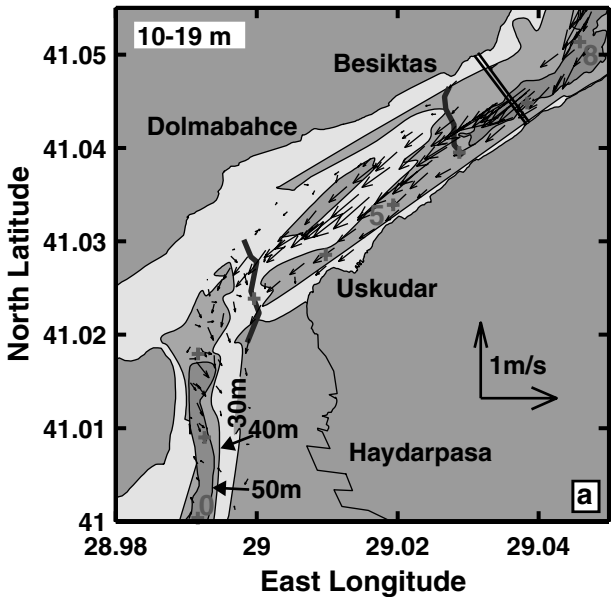

Figure 10a. All 5-min current vectors in the southern strait, averaged vertically between 10 and 19 m, which are the depths detected with the ADCP that were in the southward flow. Southward transport appeared to decrease approaching the sill crest as the flow rose above the shallowest ADCP bin. Following the direction of the channel north of 8 km, most of the flow was on the Asian side of the channel. Vectors on the European side are so small that they are barely visible. They reflect the weak flow within the zone of separated flow beginning near Beşiktaş, extending past Dolmabahçe. The dark blue lines at 3 and 6 km show the cross-strait sections plotted in Figures 11 and 12.

particular characteristics of South Sill affecting the flow are sharp channel bends at both ends and lateral variations in bottom depth. The axis of the Marmara entrance (0 km) is north-south, but at 2 km the strait turns sharply to +60°. North of the bend, the channel is straight with parallel sides 1 km apart until 8 km, where the axis turns to +10°. *Gökacsan et al.* [1997] identify an active fault running along the steep Asian coast north of Üsküdar to the bend at 8 km where it is intersected by another fault. Motion on the fault depresses the floor of the strait and moves it northeast relative to the coast.

[52] Most of South Sill is 30–40 m deep, but a central ridge rises to 28 m between Dolmabahçe and Üsküdar (Figure 9). Narrow channels from the north cut into the northern side of the sill on opposite sides of the ridge. Seismic profiles show that the eastern channel is the remnant of a paleovalley formed during the last glaciation and subsequently covered by more recent sediments. The sill crest extends north-south for 1500 m from shoals off Üsküdar (not shown) to Dolmabahçe. The distance across the crest from it to the northern side (40-m isobaths) is 300 m along the Asian side and by 1200 m along the European side. South of Dolmabahçe the European shore turns eastward into the Golden Horn, the mouth of a river that was dammed many years ago and now has little flow.

[53] Although the flows were too swift to profile with AMP while running cross-channel sections, we used depths from the BioSonics to fill in gaps in our bathymetry. Plotted in gray, the principal one of these convinced us that there is no gap connecting the channels leading to the western side of the sill crest.

5.2. Southward Flow

[54] Velocity vectors from all of the AMP bursts were averaged vertically to form the plots in Figures 10a–10c. Southward flow entered this section following the direction of the channel north of the bend until it was deflected by the Asian shore downstream near the bridge (Figure 10a). Speeds were highest on the Asian side, as also observed in the composite cross-channel section near 6 km (Figure 11). The very weak shallow flow in the western half of the channel, barely visible in Figure 10a, is the signature of a well-known, slowly rotating eddy extending well past Dolmabahçe from Beşiktaş. It results from the separation of the surface flow from the European side downstream of the bend. So much debris collected in the eddy that we were not able to complete AMP bursts through it, and consequently, we failed to sample the western side of the sill adequately.

[55] Concentrated in the eastern half of the channel, the southward flow continued to thin as it approached the sill. Although the zero isotach remained near 20 m on the sill crest (Figure 12), the same depth found at 6 km, the total transport we could measure rapidly diminished as more of the flow rose above the shallowest ADCP bin. This is evident in the progressive disappearance of flow vectors in Figure 10a and in the large contrast in southward transport between a composite cross-channel section north of the sill (Figure 11) and one across the southern flank of the sill. A weakly stratified surface layer extended to 10–12 m at 6 km, but over the crest we found one only on the western side. The eastern side was stratified below 2 m.

5.3. Northward Flow

[56] Most of the deep flow comes up to Marmara Channel, which directs it over the western part of the sill, although the distance over the eastern part is much shorter (Figures 10b and 10c). Nearly all of the northward transport was beneath the deepest ADCP bin on the crest, but some of it reappeared off Beşiktaş as it left the narrow channel along the western side. Some northward flow, however, spilled into the narrow channel along the eastern side and merged with the western component just north of the sill, between 5 and 6 km. It appears, though, that most of the dense water crosses the sill beneath or close to the zone of separated flow and hence is closer to being a simple reduced gravity flow of one layer than an exchange flow.

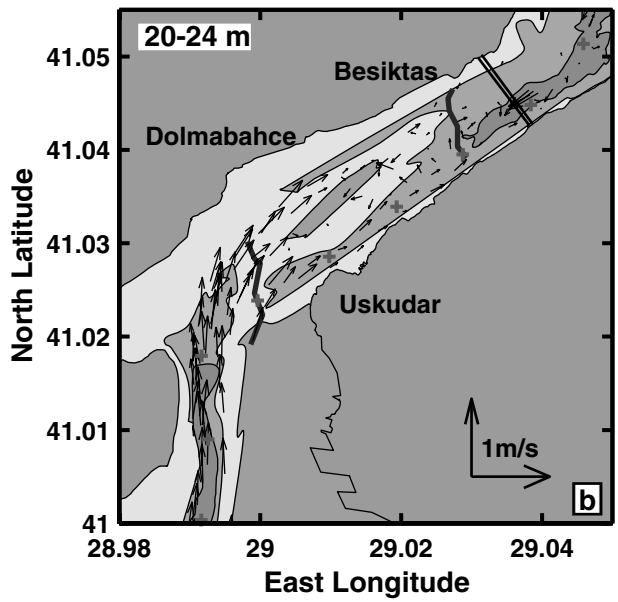

Figure 10b. Five-minute average current vectors between 20 and 24 m.

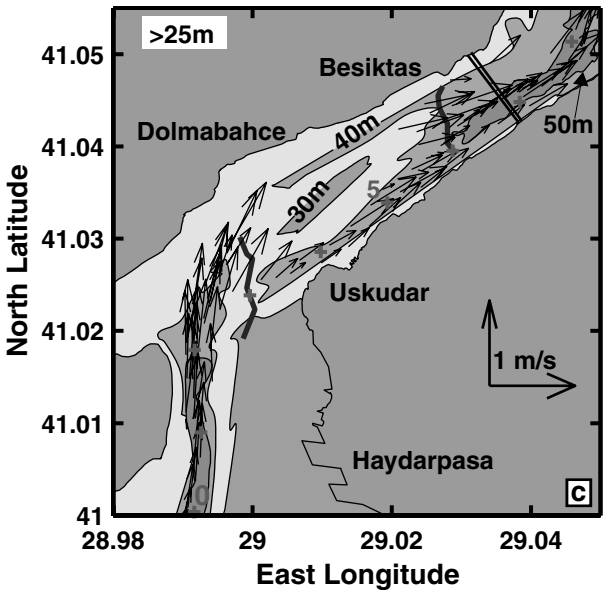

Figure 10c. Five-minute average current vectors 25 m and deeper. Flow over the western part of the sill appeared to vanish approaching the sill crest as it went below the deepest ADCP bin.

[57] We came closest to following a streamline with the dominant flow during burst 10, which passed over the European side of the crest (Figure 9). Unfortunately, the run ended prematurely in the shallow recirculation cell off Dolmabahçe, where large debris wrapped around the profiler to double its "added mass." More than half of the interface moved northward, but most of the transport was in a homogenous bottom layer (Figure 13). The maximum velocity we measured approaching the crest was 0.8 m s^{-1}, which extrapolates to slightly more than 1 m s^{-1} on the crest using continuity. The interface varied rapidly over the sill, but it always contained at least one weakly stratified layer and sometimes two. Near the crest these layers were up to 5 m thick and occupied a significant fraction of the interface.

[58] Although water with $\sigma_\theta \geq 28.8$ was shallower than the crest south of the sill, the maximum density crossing over was only 28.6. North of the sill, burst 12 found densities >28.2 but not 28.4, confirming that mixing generated at the sill must have entrained water from the interface to dilute the homogenous bottom layer. This mixing also removed most of the temperature minimum from the northward water; comparing θS relations, $\sigma_\theta > 21$ across the sill (Figure 14). On the north side (5.5 km), the deepest water was less dense than on the south side and was mixed along line A. Slightly less dense water mixed along line B and so on successively to line C. There was very little of this water, and it likely was produced by mixing of an intermediate product. Overturns within the bottom layer are evident in Figure 13 and were confirmed by plotting profiles on an expanded scale (not shown here). These signatures are direct evidence for the mixing we inferred from the salinity changes.

5.4. Hydraulic Control

[59] In terms of the transports, $\overline{Q_S} = \overline{u}_1 w h_1$ and $\overline{Q_N} = \overline{u}_2 w h_2$ the control condition (1) can be expressed as

$$G^2 = \frac{\overline{Q_S}^2}{g' w^2 (D - h_2)^3} + \frac{\overline{Q_N}^2}{g' w^2 h_2^3} = 1, \qquad (4)$$

where h_2 is the height of the zero isotach above the bottom and w is the width. Using the full sill width, 1500 m, gives the curves in Figure 15. Having the lower layer active requires $h_2 \leq 7$ m, compared to $h_2 = 26$ m for upper layer control. We observed $h_2 \approx 20$ m at South Sill (Figure 13), which gives $G^2 \approx 0.2$ in Figure 15.

[60] The major discrepancies with the assumptions are (1) the northward and southward flows are far from uniform laterally across the sill and (2) the interface occupies an appreciable fraction of the water column and contains significant transport. On the west side it is one third of the water column, and on the east side it is much more. Assuming that the northward flow is only 800 m across (Figure 12), $F_2^2 \geq 1$ when $h_2 \leq 10.5$ m and $u_2 \geq 1$ m s^{-1}. If the upper layer was also confined to half the channel, it could have controlled the flow if $h_1 \leq 14$ m and $u_1 \geq 1.5$ m s^{-1}. Water from the Black Sea entered the strait with $u_1 \approx -0.1$ m s^{-1}, and the pressure gauges found an average decrease in sea level of 0.32 m. Neglecting friction and applying the Bernoulli relation to streamlines in the upper layer yields

$$u_1 = -\sqrt{u_0^2 + g \times (h_2 - h_1)} = -\sqrt{0.1^2 + 0.32g} \approx -1.9\,\mathrm{m\,s^{-1}}. \qquad (5)$$

[61] Both conditions are close enough to what we observed that we cannot exclude them with available bathymetry and velocity mapping. Consequently, if we allow for a shift in the relative contributions by northward and southward flows, something close to hydraulic control is feasible. Where we could follow the north-

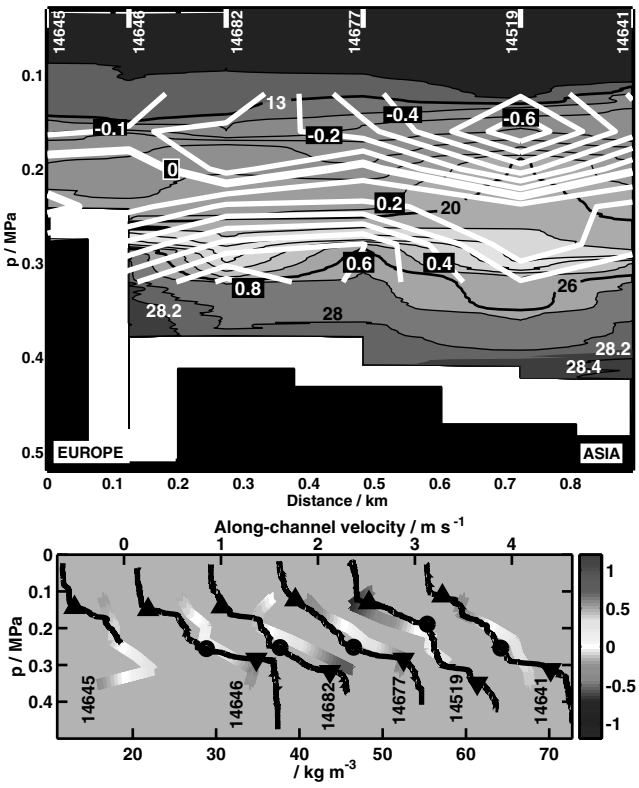

Figure 11. (top) Density and along-channel velocity contours just north of South Sill, near 6 km. Positions of this composite section are plotted in dark blue in Figure 10a. (bottom) Density and velocity profiles used in the contours in Figure 11 (top). Symbols on the density profiles mark the top, middle, and bottom of the interface, as defined in section 4.3. Color bar for velocity is at the right.

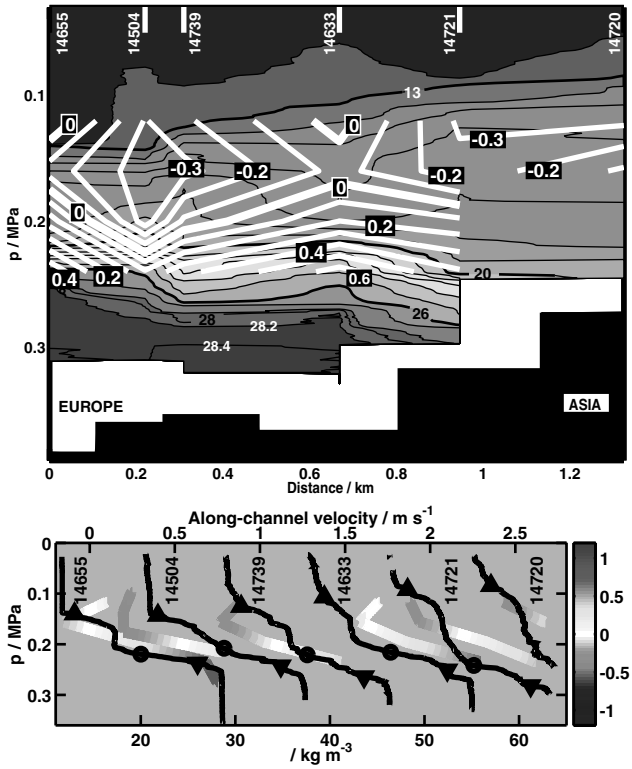

Figure 12. (top) Density and along-channel velocity contours across the southern flank of South Sill near 3 km, along the tracks plotted in dark blue in Figure 10a. The central profile, AMP14633, was close to the 3-km position on the thalweg. Distance was computed from the western profile, AMP14655. (bottom) Density and velocity profiles used to make the contours.

ward flow over the sill, for example, burst 12, we found dips and rebounds of isopycnals similar to those found downstream of hydraulic controls on sills. These are further indications that at least some parts of the flows are controlled.

5.5. Summary

[62] Bends in the channel north and south of the sill direct most of the upper and lower flows to opposite sides of the channel as they cross the sill. This results in much of the northward transport passing under a sluggish recirculation cell along the European side. The interface occupied a large fraction of the water column over the sill and included most of the water flowing south. Crossing the sill produced large overturns in the bottom layer, which entrained the lower part of the northward flowing interface to produce the first rapid dilution of the bottom water. The mixing was so intense that it nearly linearized the θS relation of $\sigma_\theta > 21$, removing most of the incoming temperature minimum. Because major portions of lower and upper flows were too thin to be detected by the ship's ADCP, hydraulic control was estimated using the average transports in a two-layer formulation based on average transports, width, and interface height. Control is feasible, but it is likely that relative contributions from the two layers varied laterally across the sill crest.

6. The Contraction, the Hole, and the Bend

[63] *Oğuz et al.* [1990] identified the contraction as an important hydraulic control, and our first runs showed the interface thickening and rising at the exit. To define the characteristics of this important section, we ran six AMP bursts through it. Three of the bursts, 6–8, and several cross-strait runs were taken in rapid sequence between yeardays 251.88 and 252.05. We could not drop AMP while crossing the channel but examined the bathymetry and backscattering surfaces with the BioSonics. Owing to the short elapsed time, 4.2 hours, these sections provided a nearly synoptic three-dimensional view. Burst 6 followed the 50-m isobath on the Asian side, burst 8 went along the European side, and burst 7 was down the middle (Figure 16). During the 3 hours prior to burst 6 the sea level difference between Anadolukavagi and Fenerbahçe dropped from 0.42 to 0.30 m (GOL; Figure 3). This had little effect on the deep flow, as current meter 4016 decreased only from 0.95 to 0.86 m s^{-1} and CM4819 remained between 0.66 and 0.60 m s^{-1}.

6.1. Bathymetry

[64] Constructed with the aid of BioSonics bottom soundings, the bathymetry in Figure 16 shows a large "hole" immediately

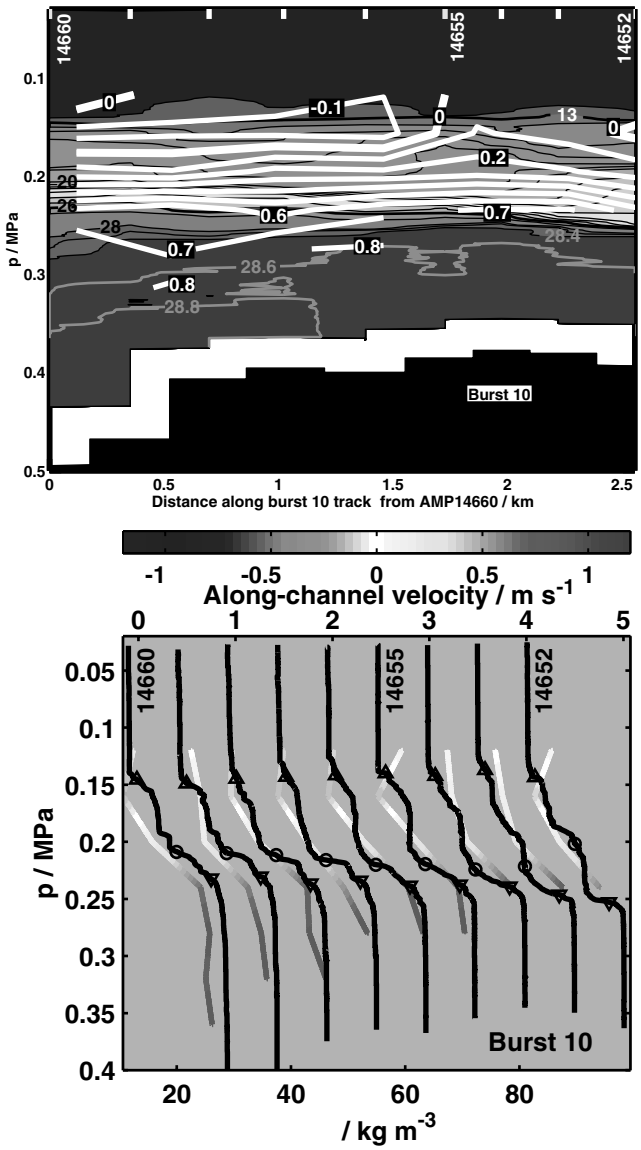

Figure 13. Contours for burst 10, which passed over South Sill from the Marmara Channel to the southern end of the channel on the western side of South Sill. The ship track is plotted in Figure 9.

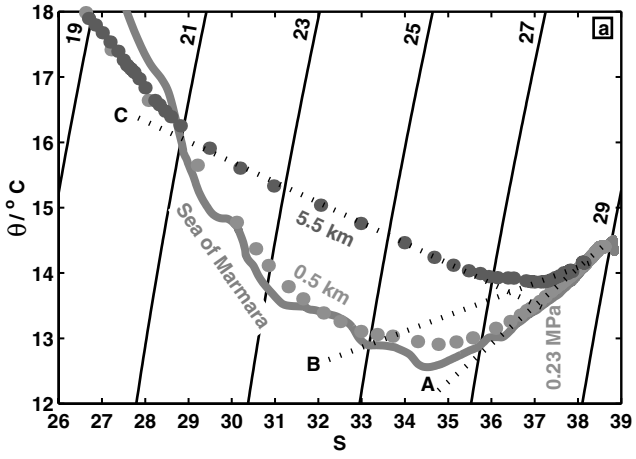

Figure 14. Change in average θ*S* relations of the deep northward flow from the Marmara entrance channel (0.5 km) to north of South Sill (5.5 km). The mixing had to occur in successive stages, some of which are plotted as black dashed lines A, B, and C, and finally involved the lower part of the interface.

south of the contraction, which is not on the standard chart. The bottom begins deepening in the middle of the contraction, slightly exceeds 100 m off Kandilli at 10.8 km, and then shoals in the reverse bend. Between 12 and 9 km it is a significant fraction of the cross-sectional area (Figure 5). *Gökacsan et al.* [1997] show that the bends result from an active fault running SW-NE through Bebek offsetting a N-S fault tangent to the European coast at Rumelihisar and Arnavutköy. The channel side of the fault has moved downward.

[65] The shape of the channel changes from a broad "U" with a flat bottom in the contraction (Figure 17a), to a steep "V" with one-fifth slopes in the hole (Figure 17b). As the depth gradually rises farther south, the channel floor flattens until it encounters a deep ridge with a notch at 8.2 km. The bathymetry shows the ridge extending from the Asian shore but does not indicate the narrowness of the passage. Our cross-channel line S happened to cross it and revealed a 100 m wide gap in steep r idges extending from both shores (Figure 17c). Along-channel runs show that the ridge is narrow, at least on the Asian side, and strongly affects the flow (Figure 18).

6.2. Evolution of the Flow

[66] To examine how the southward and northward flows evolved, Figures 19a and 19b show all of our ADCP data; each vector is an average over 5 min and the depth intervals shown on the plots. The only cross sections of velocity are included in Figures 17a–17c. Additional insight comes from overlaying contours of along-channel velocity on density and on the acoustic images taken during bursts 6, 7, and 8 (Figure 20). The tracks of these runs are plotted in Figure 16.

6.2.1. Southward flow. [67] After accelerating and decelerating in the northern half of the strait the southward flow accelerated steadily after entering the contraction at 15 km (Figure 3). At Rumelihisar its speed was relatively uniform laterally in the central 500 m of the channel and slowed near the edges (Figure 17a). The direction was southward in the center and somewhat westward toward the Asian side. The zero isotach rose slightly from 0.31 MPa in the east to 0.28 MPa in the west.

[68] South of Rumelihisar the flow separated from the European side where the coast turned sharply westward. The separation formed a narrow shear line clearly visible from shore and produced a slowly moving backwater over the broad shoals between Bebek and Arnavutköy (Figure 19a). The flow then impinged against the eastern shore at Kandilli and was deflected across the channel, separating from the Asian coast between Kandilli and Vaniköy. Just north of the separation, burst 6 found peak velocities >-0.6 m s^{-1} (Figure 20 (top)). Isopycnals rose steeply with the decreasing isotachs on the shoreward side of the velocity maximum. Within the separation zone, velocities were so small that most of their vectors cannot be seen on the plot.

[69] As it crossed the channel from Kandilli, the flow broadened until it was redirected eastward by the point at Arnuvatöy, as shown by bursts 7 and 8 velocity contours (Figure 20 (middle) and 20 (bottom)). A much weaker cross-channel component carried it back to the Asian side near Vaniköy. Although we did take measurements close to the European shore south of 10 km, the broad shoal south of the point appeared to be another large zone of sluggish separated flow. South of Vaniköy, the cross-channel component of the flow decayed, and by 9 km most of the flow ran approximately parallel to the channel, and the peak velocities decreased as the shallow isobaths moved apart. Throughout this section the zero isotach rose from ≈ 0.28 to ≈ 0.20 MPa.

6.2.2. Northward flow. [70] At 8 km the upper part of the northward flowing interface extended from the steep Asian coast across the wide and gently sloping European side (Figure 9). Nearly all of the homogenous bottom layer was in a channel 70 m deep and 300 m wide between the 50 m isobaths. The constriction at 8.2 km appears to reduce cross-sectional area below 50 m by at least half before the channel continues deepening and widening to north. The vectors in Figure 19b show the vertically averaged flow being deflected eastward through the notch. As evident in Figure 18 flow over a side of the notch responded strongly. The lower half of the interface was overturning, and the zone of intense backscatter on the lee side is a signature often seen at hydraulic controls.

[71] Owing to the rough topography along the channel, similar indications of hydraulic responses were also found farther north along both sides of the channel (Figure 20 (top) and 20 (bottom)). The responses at 9.2 km in burst 6 (Asian side) and 9–10 km in burst 8 (European side) occurred at submerged projections of prominent points in the coastline. We do not know how much these features constricted the deep flow because the bathymetry is inadequate, and we did not run cross-channel sections over them. It is clear, however, that these features produced significant responses and that the deep flow separated from the sides of the channel downstream of the projections. As found earlier with the upper

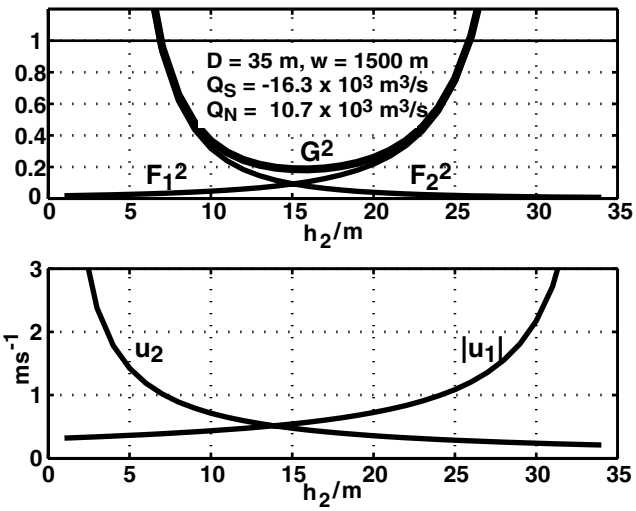

Figure 15. Evaluation of (4) for the observed transports with the full depth D and width w of South Sill crest. Here h_2 in the height of the zero isotach above the bottom.

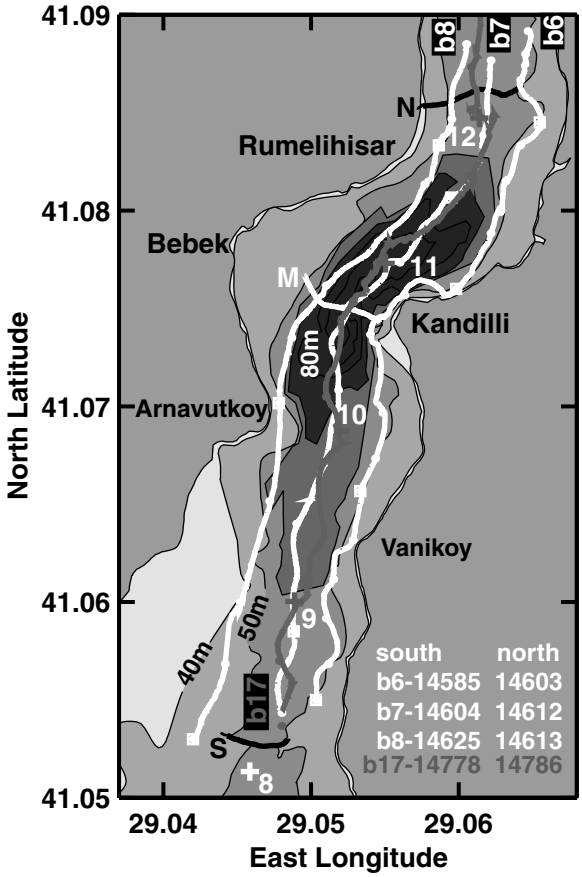

Figure 16. Bathymetry and data locations through the region of intense mixing and possible hydraulic control beginning in the south end of the contraction, which is between 11 and 14 km. Ship tracks of bursts 6, 7, and 8 are white, and burst 17 is maroon. Drops are marked with dots, and multiples of 5 are squares. N, M, and S show the tracks of cross-channel BioSonics sections. Line S ran along what our measurements show to be a thin sill with a notch near the center of the channel.

flow, most of the velocity vectors in the deep separation zones north of Vaniköy on the Asian side and Arnavutköy on the European side are too small to be seen in Figure 19b. Density contours within the lower layer oscillated wildly between 8 and 10 km, apparently in response to the ridge at 8.2 km (Figure 3). During these oscillations the bottom layer freshened and the salinity of the northward flowing interface increased even more (Figure 7). Both the oscillations and the mixing seem to be results of the large perturbations caused by flowing through the deep constriction at 8.2 km and over the other sidewall projections north.

[72] Passing over the hole decelerated the flow and drew down the lower layer (Figure 20 (middle)). The flow regained its speed on the north side, and the rebounding isopycnals had even larger vertical excursions than were found south of the hole. Large overturns (not shown here) indicated mixing between the lower part of the interface and the lower layer.

[73] The core of the deep northward flow continued past Kandalli before being deflected eastward by contact with the coast south of Rumilihisar. We infer that some of this water upwelled near the Asian side to produce the upward tilt in the interface.

6.2.3. Tilting and thickening of the interface. [74] To examine changes in the interface through this section, Figure 21 shows the depths of three isopycnals, σ_θ = 13, 20, and 26, approximately marking the top, middle, and bottom of the interface. The surfaces were constructed by contouring densities from bursts 6–8, and the velocities were then interpolated vertically onto the isopycnals. The bottom surface, σ_θ = 20, had no net change in depth but generally sloped slightly upward toward the east, particularly across the Rumelihisar. The middle of the interface, σ_θ = 20, rose gradually and approximately uniformly across the channel, but it also was slightly elevated across from Rumeilhisar, indicating possible upwelling along the Asian side.

[75] The major change occurred in upper surface, σ_θ = 13, which rose 8 m over a distance of about 100 m along the eastern shore as the flow rounded Kandilli. Owing to their spacing, these contours appear to underestimate the steepness of the rise, as is evident by comparing with cross-channel line M (Figure 19b), which shows the greatest thickening within the point. The rise occured progressively farther south across the channel and was found slightly south of Arnavutköy during burst 8. Resulting from thickening of the upper interface, the front appeared to be the subsurface expression of the separation zone and extended fully across the channel. Flow on the upper boundary of the interface apparently followed the curving depth contours of the front.

6.3. Mixing

[76] Because the θS relations were linear north and south of the hole, we could not use them to determine whether new water types were being created. The acoustic records, however, contain nearly continuous images of mixing (Figure 20). These appear as thick, orange backscattering surfaces in Figure 20 and slope upward where σ_θ turns up in the matching density contours. Strong returns came throughout the water column, but the most intense were in the southward flowing interface along the separation front and contain signatures of overturning billows.

[77] The images in Figure 20 are too compressed to show the billows, but the region in the box in burst 7 is replotted on an expanded scale in Figure 22. On the upper scattering surface near 10.8 km are characteristic "braids" found in radar backscatter from atmospheric billows and some of our earlier measurements in mixing areas [*Seim and Gregg*, 1994]. Because burst 7 cut through

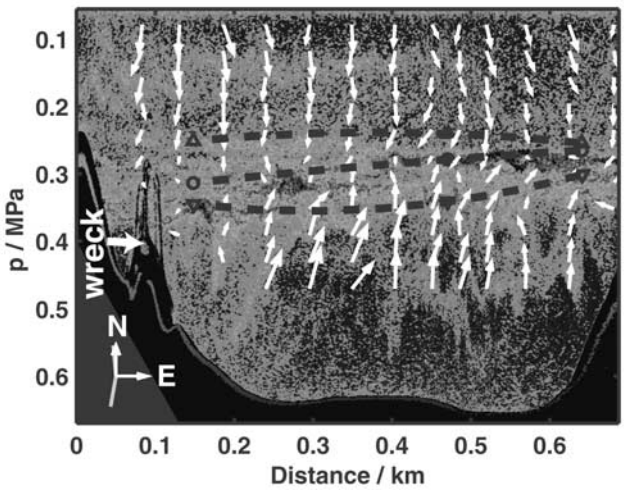

Figure 17a. BioSonics image and ADCP velocities taken while crossing the channel on the N (north) of Figure 16, near Rumeilhisar. Arrows are upward for northward flow and to the right for eastward flow. Dashed lines mark σ_θ = 13, 20, and 26 kg m^{-3} observed in along-channel runs during bursts 6–9; dashed lines connect the symbols as approximate indicators of the interface. The wreck on the east side is not charted.

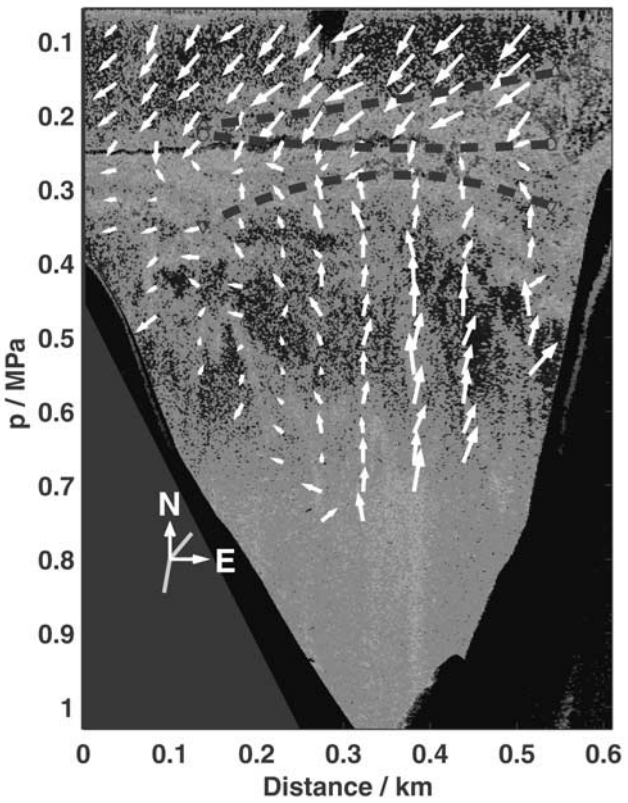

Figure 17b. Across the channel on the M (middle) track, over the center of the hole off Kandili.

the front and did not follow streamlines along it, we cannot examine the full evolution of the instabilities but note that they were thinner than 1 m when first visible. They grew rapidly and coalesced with others on the middle surface to form billows 5 m thick at 10.8 km. Farther south, at 9.5 km, burst 8 found billows grow to 10 m (Figure 20 (bottom left)).

[78] Across a density step the bulk Richardson number is

$$Ri_{\Delta} = \frac{g'\Delta z}{(\Delta u)^2}, \tag{6}$$

where Δz is the thickness and Δu is the velocity difference. We have good estimates of g' and Δz because the AMP dropped rapidly and captured nearly instantaneous states of the density interface. The velocity estimates, however, are strongly smoothed vertically by the ADCP, which was set for 4-m bins, and in time, 5 min, which corresponds to along-channel distances of at least several hundred meters. As we had consistent values for $\overline{Q_S}$ north of 9 km, the velocity magnitudes are realistic. The question is how much of the total velocity difference was across the interface where the mixing started.

[79] The acoustic images show the instabilities beginning shortly after the density interface were very compressed, as shown by the lengths of the blue and red sections of the AMP trajectories. Along the center of the channel (burst 7) $\Delta z = 7$ m in AMP14609 (Figure 22), and it was even thinner, 4 m, farther north in AMP14611 (Figure 20 (middle)). Near AMP14609, velocities were 0.4 m s^{-1} in the uper layer and 1.0 m s^{-1} in the lower. That difference across the density interface gives $Ri = 0.16 \times 4/1.4^2 = 0.32$. This is consistent with the appearance of the billows and suggests that compression of the interface by the separation front was the major factor initiating the mixing.

6.4. Hydraulic Control

[80] The thickening and abrupt rise of the upper half of the interface south of 11 km are similar to responses found in laboratory and numerical models of hydraulically controlled flows through contractions when the upper layer is active. In this case the exchange flow should have been critical or supercritical when it exited the contraction off Rumeilhisar. Cross-channel line N crossed the strait off Rumelihisar at 12.2 km and found the interface at middepth and the flow relatively uniform across an approximately rectangular channel 700 m wide and 60 m deep (Figure 17a). Using $h_2 = 32$ m in (4) yields $G^2 = 0.17$. Only when $h_2 < 12$ m or > 47 m is $G^2 \geq 1$. Because the profiles and transports were well resolved in this section (Figure 7d) and neither of the two cases appears feasible, we conclude that there was nothing resembling a conventional hydraulic at the south side of the contraction.

6.5. Summary

[81] If the section is considered as a simple contraction, the rapid entrainment of the interface at its exit is strong evidence for hydraulic control by an active upper layer. Observed velocities and layer thickness at the exit, however, are far from those needed for two-layer control. Rugged bathymetry and sharp bends make this section far more complex than a simple contraction. A cross-channel ridge, numerous smaller projections, and a steep-sided hole perturb the northward flow, which did not experience a detectable net acceleration, consistent with the absence of a constriction in the deep cross-sectional area. Strong cross-channel circulations and major flow separations affected the southward flow in addition to a net acceleration. The rapid thinning of the homogenous surface layer and thickening of the interface occured

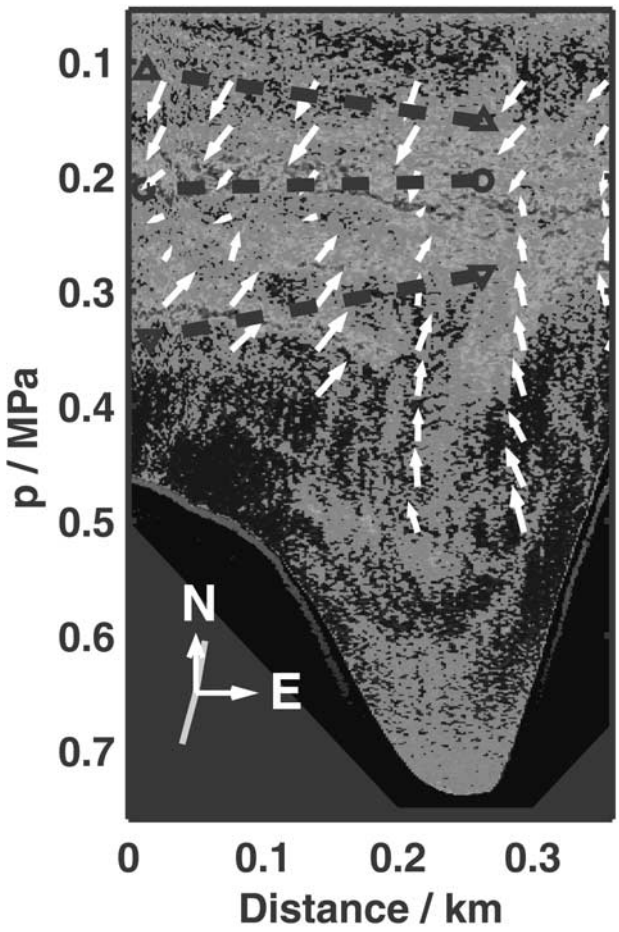

Figure 17c. Across the channel on the S (south) track, showing the deep constriction. The image suggests that a strong downwelling disrupted the lower interface and that some of the downwelled water rose along the sides of the notch.

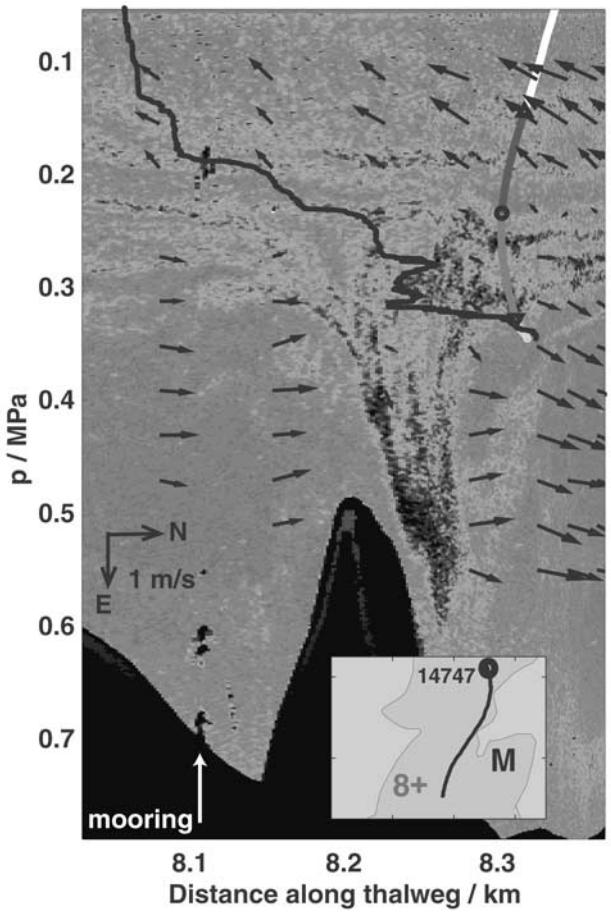

Figure 18. Hydraulic response of the lower layer to the deep sill at 8.2 km. Arrows showing the along-channel velocity measured during this section are superimposed on the BioSonics image, and the dark line is density in AMP14747. The colored line is the estimated AMP trajectory, with blue indicating the upper half of the interface and red indicating the lower half. On the inserted map the solid circle shows where AMP14747 was released, and the line is the ship's track before the AMP was released. The instrument was carried southward while in the upper layer before it encountered the hydraulic response. M shows the location of the mooring visible on the BioSonics image.

as the flow rounded the second of two sharp bends along a steeply curved separation zone. These features point to the importance of friction in limiting the flow. Hints of upwelling immediately north of the bend raise the possibility that centrifugal forces may be important and contribute to the mixing, as found in Tacoma Narrows by *Seim and Gregg* [1997].

7. From the Contraction to Over North Sill

[82] We did not sample the northern half of the strait as intensively as the southern because it did not appear as active until the dense outflow went over North Sill. Although the upper layer was uninteresting, that was not the case below it. The interface changed steadily north of the contraction, and the bottom layer freshened quickly as it left the strait, before having a spectacular response to North Sill.

7.1. Bathymetry

[83] The two wide bends north of the contraction take the channel through the section that was once a lake and has been subsequently offset by faulting [*Gökacsan et al.*, 1997]. Width increases to 3 km and then decreases to half that by 24 km, the northern end of the bends (Figure 5a). From 23 km through the Black Sea entrance is the longest straight section of the Bosphorus, and up to 28 km it also appears to be the smoothest. A cross section at 27.3 km shows gently sloping sides, which are 0.9 km apart at the depth of the interface, 30–40 m (Figure 23). At 28.5 km the thalweg descends to ≈90 m along a steep-sided 100 m wide channel produced by faulting [*Gökacsan et al.*, 1997].

[84] The hole ends between 30 and 31 km with a very rough bottom on the northern side (Figure 24) although we were not certain that we stayed on the thalweg. After rising steeply from the hole, near 32 km the deep channel leads directly into the pre-Bosphorus channel cut into the sediments on the shelf by fluvial action. High-resolution bathymetry, taken by the NATO SACLANT laboratory [*Di Iorio and Yüce*, 1999], shows that the channel here is 400–600 m wide. Its walls diverge and descend from 30 m at 33 km to 45 m at 34.5 km, with the eastern side somewhat shallower. The channel floor gradually crests at 34.5 km but descends steeply from 35.8 to 36.6 km and then rises abruptly before resuming a gradual descent as it curves westward.

7.2. Evolution of the Flow

[85] The large variations in cross-sectional area modulated the steady acceleration of both southward and northward flows as they grew thinner (Figures 3 and 24). Between 28.5 and 30.7 km we found the homogenous bottom layer reaching velocities of 1.1–1.2 m s^{-1}. Most of the interface was moving north; some of it as a slow 20 m thick strongly stratified flow along the sides.

[86] Numerous overturns within the interface appear responsible for the interfacial mixing exhibited in Figure 6c. (To interpret the θS evolution, it is necessary to recall that in any profile, water above the zero isotach evolved north of that position and water below it evolved farther south.) The overturns were too small to invert the σ_θ contours in Figure 24 but they are revealed by inspecting individual profiles and seem responsible for the coherent lines of strong acoustic backscatter rising from the bottom of the interface south of the hole (Figure 24). The interfacial mixing therefore was produced by a down gradient flux between two strongly stratified flows moving slowly in opposite directions, rather than by one flow entraining the other.

[87] Regions of intense backscatter were thicker and stronger in the shallower water along the sides of the hole (Figure 23 (right)), where we did not take measurements. On the right side at 30.1 km, strong returns extended from the sides along the bottom to the edge of the hole, but on the left side the backscatter began about 10 m above the bottom. This suggests a cross-channel circulation driven by bottom stress, sinking on the right and rising on the left.

[88] Large overturns within the bottom homogenous layer were apparent even south of the hole. Crossing the hole produced a slight dip and rebound within the layer and large straining within the interface. At the northern edge of the hole the turbulence extended into the bottom of the interface; overturns up to 5 m thick between $20 \leq \sigma_\theta \leq 26$ are evident 31 km in Figure 24. The large overturns appeared to entrain water from the interface that was rapidly homogenized, terminating isopycnals with $27.8 \leq \sigma_\theta \leq 27$ in the bottom over and downstream of the hole.

[89] As the northward flow left the Bosphorus, it changed from being the lower half of an exchange flow in a strait to a reduced gravity density current confined to a channel cut into a continental shelf. The strongly stratified shelf water was flowing eastward, to the right of the density current, at 0.1 m s^{-1} [*Gregg and Özsoy*, 1999]. BioSonics images from runs across the channel showed some of the upper interface being "blown off" by the eastward rim current. Approaching the crest, we measured speeds up to 0.9 m s^{-1}. Integrating this profile with cross-sectional areas from the SACLANT bathymetry and extrapolating the deepest data to 5 m above the bottom gives $Q_n = 9.7 \times 10^3$ m^3 s^{-1}, 9% less than $\overline{Q_n}$ in the strait. Most of the northward flow over the crest was too close

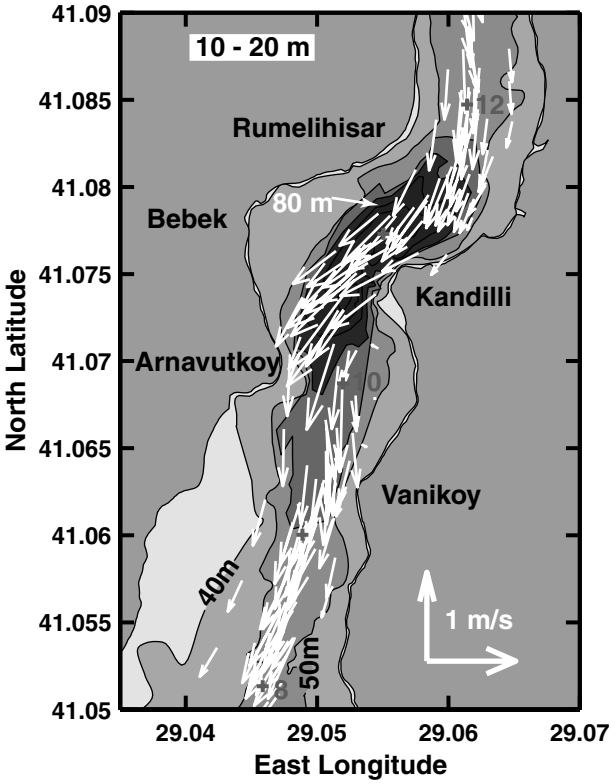

Figure 19a. Five-minute averages of the southward flow through the contraction.

to the bottom to be detected with the ADCP. Applying continuity, lower layer speeds at the crest were 15% greater than at AMP14870, or at least 1.04 m s^{-1}.

[90] Approaching the crest rapidly compressed the lower part of the interface, producing continuous billows (Figure 25). As they grew to 5 m, the billows produced density inversions and a 3 m thick homogenous layer in AMP1473. Apparently the layer was rapidly sheared because the next profile showed a smooth interface, while the BioSonics revealed another train of billows beginning to grow. They reached 7 m on the far side of crest. The activity intensified as the depth increased, culminating on a sharp isopycnal rebound at 37 km that is the signature of a hydraulic jump. Immediately downstream of the beginning of the rebound, below $\sigma_\theta = 20$, AMP14883 found 10 and 5 m homogenous layers over a 5 m overturn. These too were rapidly sheared, leaving much smoother profiles in a few hundred meters. Rapid entrainment by the bottom layer downstream of the jump terminated $\sigma_\theta = 26$ by 39 km.

7.3. Hydraulics

[91] For the reduced gravity flow in the channel, only the stratification capping the bottom layer should affect the dynamics. The density profiles in Figure 25 indicate $g' \approx 0.08$. For the estimated transport and channel width, $G^2 = 1$ when $h_2 \geq 15$ m and $u_2 \geq 1.1$ m s^{-1}. These values are essentially those extrapolated from observations before the crest and indicate a simple hydraulic control at the crest, which is confirmed by the hydraulic jump downstream.

7.4. Summary

[92] Velocities responded to the large differences in area without producing other obvious responses. Mixing was strong, but it was nearly all within the interface. After leaving the Bosphorus the dense northward flow was confined into a narrow channel that rose to a crest 4.5 km across the shelf. The reduced gravity flow was hydraulically controlled at the crest.

8. Summary

[93] During early September 1994, winds were light, and the exchange flow through the Bosphorus was gently modulated by the sea level in the Sea of Marmara in response to synoptic weather systems with periods of 3–5 days. Owing to the quasi-steady conditions, we were able to make repeated detailed observations at key sites and find conditions to be similar from one day to the next. Our principal findings are as follows.

8.1. Bathymetry

[94] As expected for a long, narrow, and shallow strait, bathymetric irregularities had large effects on the flow. These the Bosphorus has in abundance owing to complex faulting of its channel. Points, embayments, and sharp bends in the coastlines produced many flow separations. In some places the topography deflected much of the flow across the channel or concentrated the transport on one side. The most important example was over South Sill, where the principal northward and southward flows followed opposite coasts. Owing to changes in channel shape, the contraction is the narrowest part of the strait without being a minimum in cross-sectional area. It accelerated the upper layer but not the lower. Several small ridges partially obstructed the lower layer, producing responses likely to exert significant drag on the lower layer.

8.2. Stratification and the Interface

[95] With a reduced gravity of $g' = 0.13–0.16$ the interface was very strongly stratified. Never thinner than 17 m, it occupied 28–75% of water column and in many places was too thick to justify the two-layer approximation. It carried large fractions of the transport, for example, half of the dense outflow from the Bosphorus was in the interface, as was 20% of the light inflow.

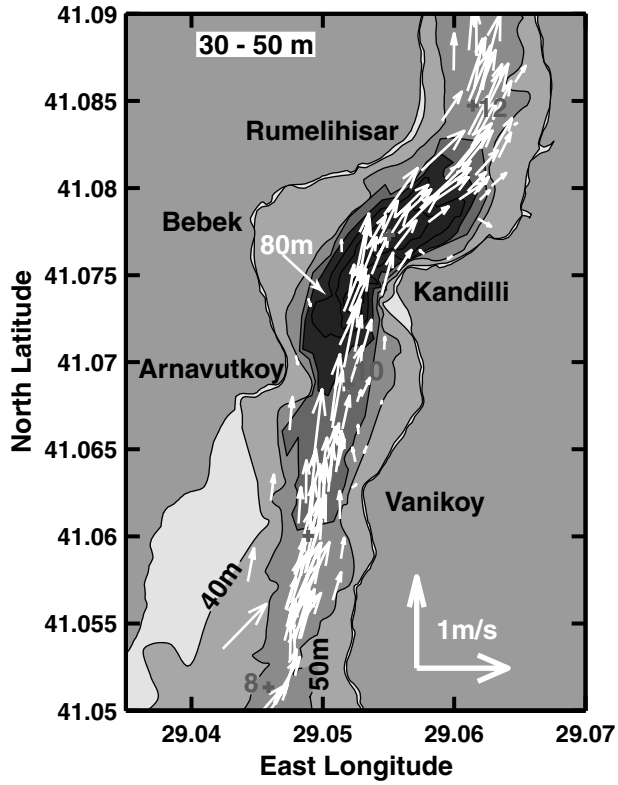

Figure 19b. Five-minute averages of the northward flow through the contraction.

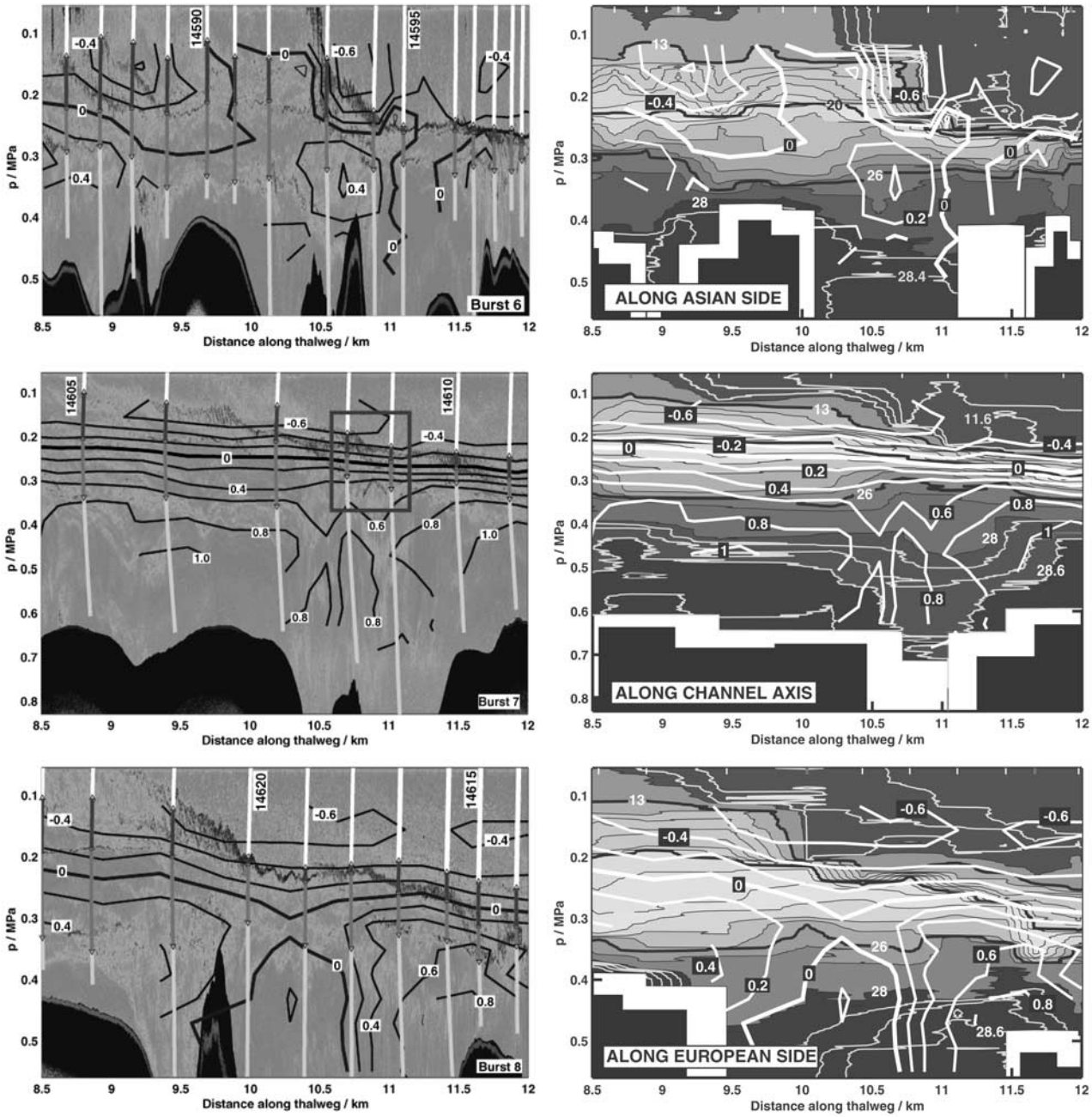

Figure 20. Images and density contours of bursts 6, 7, and 8 going south from the south end of the contraction. Contours of along-channel velocity are overlaid in black on the images and in white on the density contours. Density is contoured in intervals of 1 kg m^{-3}, except $\sigma_\theta < 12$ and $\sigma_\theta > 28$, where the intervals are 0.2 kg m^{-3} and the contours are yellow. Isopycnals used to contour the top ($\sigma_\theta = 13$), middle ($\sigma_\theta = 20$), and bottom ($\sigma_\theta = 26$) of the interface are thickened.

8.3. Transports

[96] Multiplying 1-km averages of cross-sectional area and velocity yielded averages of northward and southward transport along the strait. Averaging these gave $\overline{Q_s} = -16.2 \times 10^3$ m^3 s^{-1} and $\overline{Q_N} = 11.0 \times 10^3$ m^3 s^{-1}. Large errors occurred where much of the flow was off the channel axis or too thin to be detected by the ADCP. Although the northward transport was significantly smaller, it was considerably faster, $\overline{u}_2 \approx 0.5$ m s^{-1}, and transited in 16 hours compared to $\overline{u}_2 \approx 0.2$ m s^{-1} and 30–40 hours for the southward flow. The uncertainty results from our underestimation of $\overline{u}_1$ where the upper layer thinned rapidly south of the contraction.

8.4. Evolution of the Southward Flow

[97] The Black Sea inflow entered with two layers: a nearly homogenous surface layer extending to 0.25 MPa with $S = 17.6$ and $\sigma_\theta = 10.4$ and the nearly homogenous CIW with salinity increasing from 18.3 to 18.5 and $\sigma_\theta = 14$ to 14.4. The primary stratification resulted from temperature decreasing from 24°C at the surface to 8°C at the core of the CIW.

[98] Before reaching the contraction the flow accelerated and decelerated several times in response to changes in cross-sectional area of the channel. The surface layer thinned slightly and mixed slowly with the top of the interface as the southward flowing

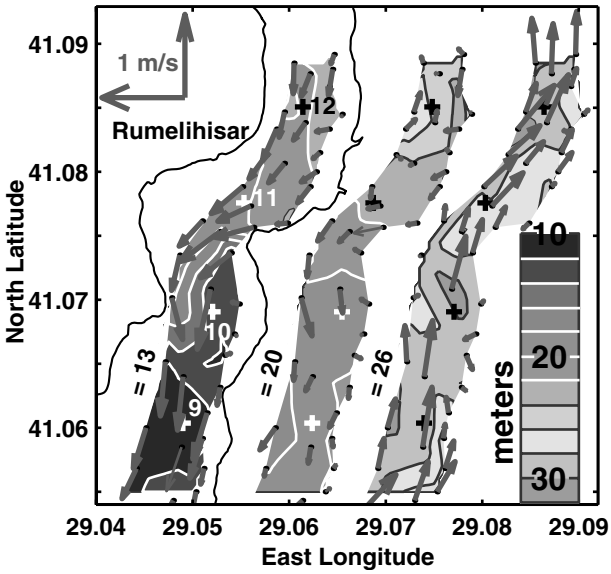

Figure 21. Depths of the top (σ_θ = 13), middle (σ_θ = 20), and bottom (σ_θ = 26) of the interface exiting the contraction. Densities were interpolated from AMP bursts 6, 7, and 8 and contoured at 2-m intervals. Five-minute velocities were interpolated onto the density surfaces.

interface mixed vigorously with the northward flow and linearized the θS relation before entering the contraction. Passing through the contraction produced the strongest acceleration, but the major response occurred as the southward flow encountered the abrupt bend and irregular topography immediately downstream. The flow separated from the European side south of Rumelihisar and from the Asian side south of Kandilli, resulting in a strong across-channel component. Close to the Asian side, there was evidence of either upwelling or a thin countercurrent, and growing billows observed downstream of Kandilli coincided with a rapid thinning of the surface layer and a thickening of the upper interface.

[99] As a result of the thinning, much of the southward transport farther downstream was too shallow to be detected with the ship's ADCP, although it was evident that the flow was concentrated along the Asian side as it went over South Sill. The southward flow was fully stratified as it exited the Bosphorus into the Sea of Marmara.

8.5. Evolution of the Northward Flow

[100] Water entered from the Sea of Marmara below 0.2 MPa and was strongly stratified to 0.3 MPa. A well-mixed bottom boundary layer with σ_θ = 28.92 kg m^{-3} contained salinities up to S = 38.5. The Marmara water flowed north in a gradually narrowing and shoaling channel. Most of the channel's discharge continued in the same direction across South Sill under a large, nearly stagnant eddy formed by a separation of the southward flow from the European side. Some water, however, passed over the Asian side of the sill, beneath the bulk of the southward flow, and spilled into the narrow bottom channel close to shore.

[101] Crossing the sill generated intense turbulence within the homogenous bottom layer. Continuing downstream, the turbulence entrained water from the bottom of the interface, reducing the bottom density by about 0.5 kg m^{-3}. Although there did not appear to be a net acceleration of the bottom layer through the contraction, turning the sharp bend, dipping into the hole, and rebounding generated intense overturning that entrained water from the bottom of the interface, reducing the density to 28.2 kg m^{-3} by the north end of the contraction.

[102] In spite of the very rough bottom, there was little change in the lower layer through the northern half of the strait. The northward flowing interface, however, mixed strongly with the upper half of the interface, reducing its average salinity by 5–6 parts per thousand. Crossing over a second steep hole at the north end with a speed of 1 m s^{-1} generated another burst of strong mixing between the lower layer and its capping interface. By 32 km, within the pre-Bosphorus channel the density of the lower layer was reduced to 27 kg m^{-3}. Some water from the stratified top of the northward flow spilled over the sides of the channel or was blown off by the lateral shear from currents on the Black Sea shelf. As the dense water approached the crest of North Sill, it was capped by an interface 3–5 m thick with $\Delta\sigma_\theta$ = 8–12 kg m^{-3}. The layer thinned appreciably in passing over the North Sill, which generated further mixing, diluting the lower layer for several kilometers downstream.

8.6. Hydraulic Controls

[103] Our understanding is based on comparisons of the observations with two-layer hydraulic theory.

1. The dense outflow from the Bosphorus was controlled at the crest of North Sill. The control, however, occurred outside the strait, where the outflow was mostly confined to a narrow channel

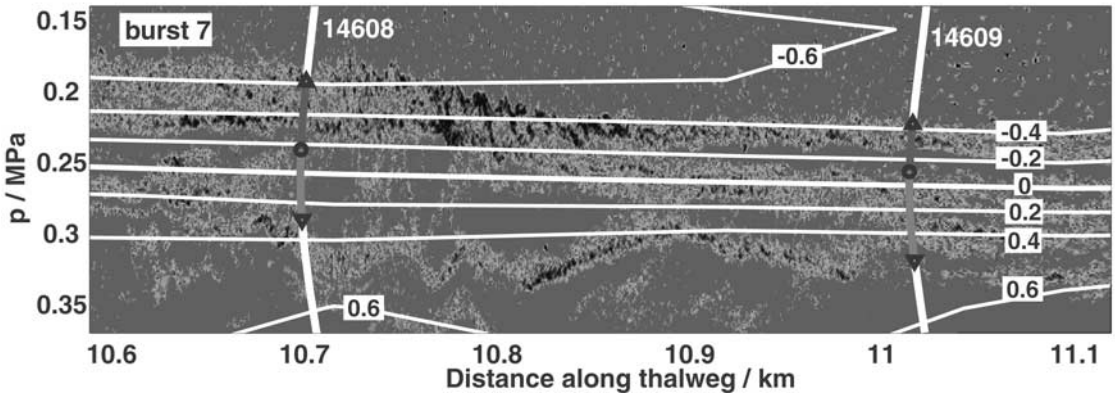

Figure 22. Acoustic images, AMP profiles, and speed contours showing billows in burst 7. This is an expanded view of the marked section on the burst 7 BioSonics record in Figure 20.

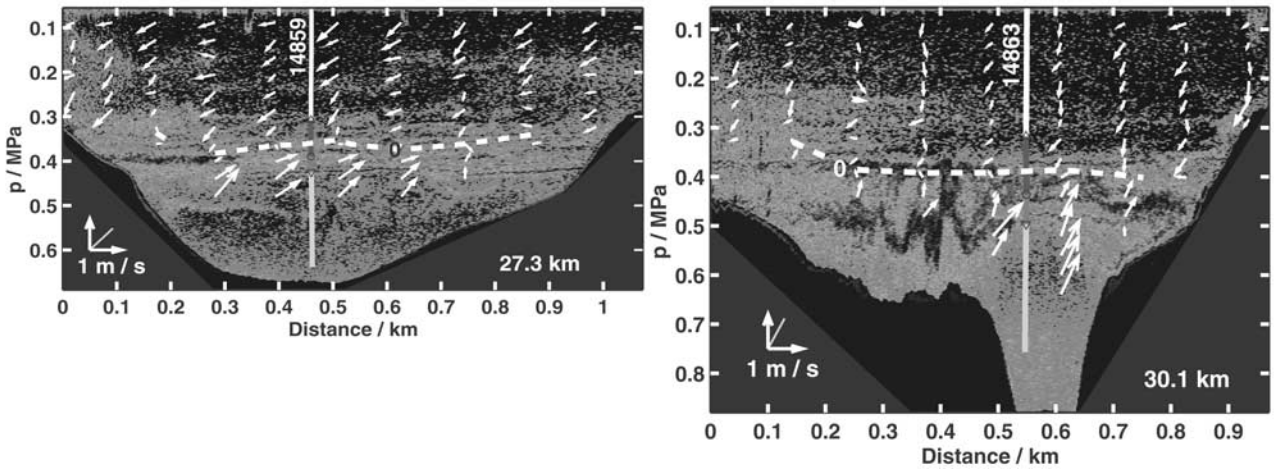

Figure 23. Cross-channel sections at (left) 27.3 and (right) 30.1 km illustrate the abrupt change in shape near the northern end of the strait. Intense backscatter in the northern cross section indicates strong mixing over the shallower regions bordering the deep channel.

cut into the Black Sea shelf. Water overhead flowed across the channel as part of the rim current. The dynamics may have been more those of a reduced gravity current than the lower half of an exchange flow.

2. The exchange flow was probably controlled at the crest of South Sill, but we could not demonstrate it because too much of the flow escaped detection with the ADCP. The control is unusual in that the flow varies strongly across the sill width. Although the lower layer is certainly active on the west side, the upper layer may be active on the east side.

3. Rapid entrainment of the interface by the upper layer downstream of the contraction strongly suggests a control in the contraction with an active upper layer. We, however, had good velocity measurements at the exit, and they exclude a two-layer control. The situation is complicated by a steep hole and two sharp bends south of the exit. The intense upper layer mixing characterizing this section occurs progressively along the curved separation surface extending across the channel from the second bend at Kandilli. Hence the surface clearly affected the mixing and may have produced it.

9. Discussion

[104] Conditions in the Bosphorus are far from those assumed by hydraulic theory and typical idealizations of exchange flows. Nevertheless, over South and North Sills we found controls similar to those expected for simple cases. Moreover, the deep flow must be supercritical between the crest of North Sill and the jump, and the upper layer may have been supercritical as it entered the Marmara. If it was, the system resembled a maximal hydraulic exchange with supercritical flows at both ends, even though transports should have been reduced by strong friction.

[105] We see several possibilities for our greatest puzzle, the dynamics immediately south of the contraction. These are the following.

1. Bottom friction played a major role, and the modeling by *Winters and Seim* [2000] captured the essential dynamics. The strong responses to bottom irregularities evident in Figures 18 and 20 make this plausible, and the modeling offers an explanation of why we did not find the control; it occurred in such a small area that detection was very unlikely.

2. Enchanced shear along the Kandilli separation zone was primarily responsible for mixing the upper layer, perhaps with the

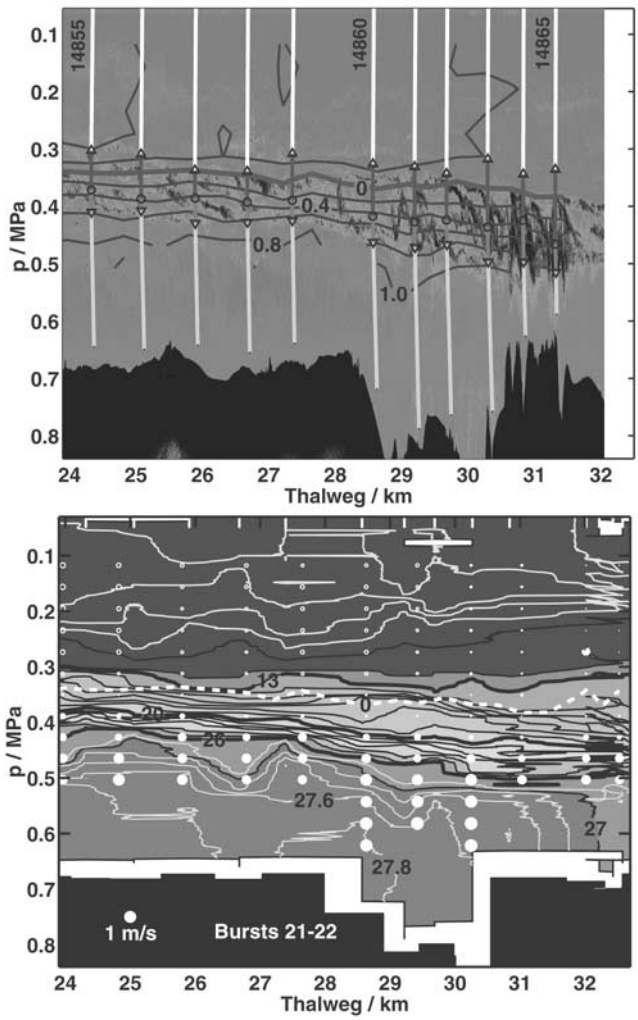

Figure 24. (top) Density and (bottom) velocity in the straight section from the last bend to the Black Sea exit. Data are included from bursts 21 and 22, which were taken a day apart. The channel narrowed at the hole.

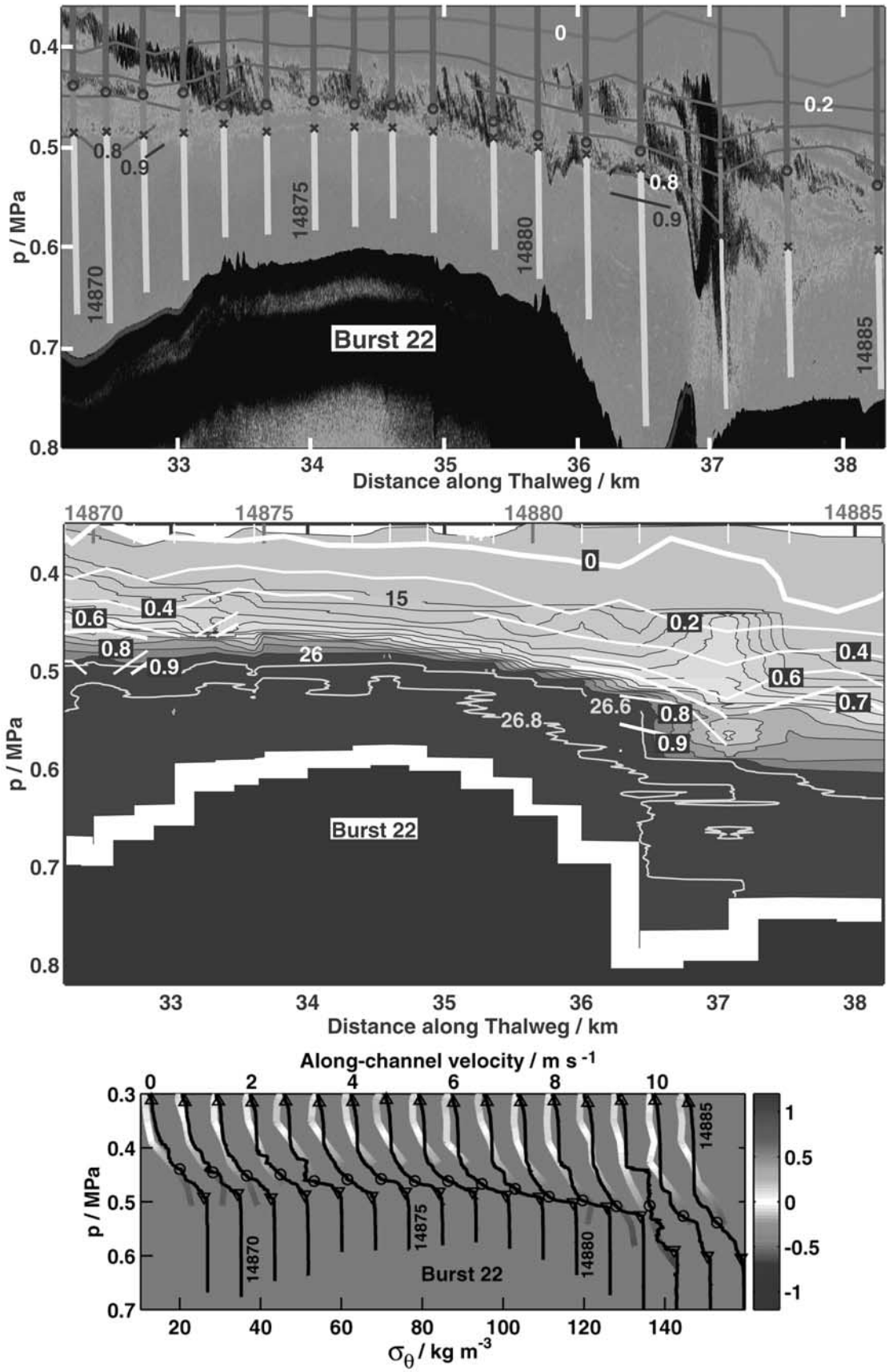

Figure 25. Burst 22 across North Sill. Billows fill the shear interface upstream of the hydraulic jump at 37 km.

aid of cross-channel circulations generated north of the bend. The separation zone was at least a factor as the onset of entraining billows followed the separation zone across the channel from the point.

3. There was a control near 8 km where the channel area seems to be slightly smaller than in the contraction and the effective width of the flow was further reduced by the separation zone off Kandilli. We did not detect the control because much of the flow was too shallow for the ADCP.

4. Responses to the contraction and South Sill were so closely coupled that they should not be considered separately. With nominal speeds of $\sqrt{g'D}$ = 3.2 m s^{-1}, long internal waves require only 30 minutes to travel the 5 km between the two constrictions.

[106] The evidence for strong bottom friction along nearly all of the strait is overwhelming, and the other possibilities are not mutually exclusive, except perhaps for possibility 3. Their relative importance is the issue. *Hogg et al.* [2001b] show how friction in a continuously stratified flow in a simple contraction can produce analogs to hydraulic controls. Owing to the complex geology of its channel, the Bosphorus has many more complications, and we probably did not find them all. At least some of the complications appear to matter, indicating that a first-order understanding is beyond present theory and ultimately will require realistic three-dimensional numerical models with accurate bathymetry. The large curvatures found over ridges and around bends call for nonhydrostatic dynamics.

[107] **Acknowledgments.** The Turkish Scientific and Technical Research Council (TÜBITAK), the Istanbul Water and Sewerage Administration (ISKI), and the U.S. Office of Naval Research funded our cruise on the R/V *Bilim*. While analyzing the data, MG has been supported by the SECNAV/CNO Chair in Oceanography. We are particularly indebted to Captain An and his crew for their skillful handling of the R/V *Bilim* in many difficult situations. Sükrü Besiktepe, Muhamed Latif, Harvey Seim, Kraig Winters, Jack Miller, Earl Krause, and Jim Turner worked hard at collecting the data with us. Dave Winkel has been very helpful with some of the data processing, Jody Klymak has shared his insights into complex flows, Seim and Winters have been generous with their modeling results and understanding, and Andy Hogg has kindly shared advanced copies of his recent work.

References

"Apollonius of Rhodes", *Jason and the Golden Fleece (The Argonautica)*, Clarendon Press, Oxford, Engl. U.K., 1993.

Armi, L., and D. M. Farmer, Maximal two-layer exchange through a contraction with barotropic net flow, *J. Fluid Mech.*, *164*, 27–51, 1986.

Armi, L., and D. Farmer, A generalization of the concept of maximal exchange in a strait, *J. Geophys. Res.*, *92*, 14,679–14,680, 1987.

Bormans, M., and C. Garrett, The effect of rotation on surface flows through the Strait of Gibraltar, *J. Phys. Oceanogr.*, *19*, 1543–1557, 1989.

Dalziel, S., Two-layer hydraulics: A Functional approach, *J. Fluid Mech.*, *223*, 135–163, 1991.

Di Iorio, D., and H. Yüce, Observations of Mediterranean flow into the Black Sea, *J. Geophys. Res.*, *104*, 3091–3108, 1999.

Farmer, D., and L. Armi, Maximal two-layer exchange over a sill and through the combination of a sill and a contraction with barotropic flow, *J. Fluid Mech.*, *164*, 53–76, 1986.

Gökacsan, E., E. Demirba, F. Oktay, B. Ecevitoğlu, M. Şimşek, and H. Yüce, On the origin of the Bosphorus, *Mar. Geol.*, *140*, 183–199, 1997.

Gregg, M. C., and E. Özsoy, Mixing on the Black Sea shelf north of the Bosphorus, *Geophys. Res. Lett.*, *26*, 1869–1872, 1999.

Gregg, M. C., E. Özsoy, and M. A. Latif, Quasi-steady exchange flow in the Bosphorus, *Geophys. Res. Lett.*, *26*, 83–86, 1999.

Helfrich, K. R., Time-dependent two-later hydraulic exchange flows, *J. Phys. Oceanogr.*, *25*, 359–373, 1995.

Hogg, A., G. Ivey, and K. Winters, Hydraulics and mixing in controlled exchange flows, *J. Geophys. Res.*, *103*, 30,696–30,711, 2001a.

Hogg, A., K. Winters, and G. Ivey, Linear internal waves and the control of stratified exchange flows, *J. Fluid Mech.*, 357–375, 2001b.

International Oceanographic Center, Istanbul Boga71, Map INT 3756, Monaco, 1985.

Lawrence, G., Can mixing in exchange flows be predicted using internal hydraulics?, in *The Physical Ocenography of Sea Straits*, edited by L. Pratt, pp. 519–536, Kluwer Acad., Norwell, Mass., 1990.

Marsigli, C. L. F., Internal observations on the Thracian Bosphorus, or true channel of Constantinople, represented in 1681 by letters to Her Majesty, Queen Christina of Sweden, in *Oceanography Concepts and History*, edited by M. B. Deacon, pp. 34–44, Stroudsburg, Pa., 1978.

Oğuz, T., E. Özsoy, M. A. Latif, H. I. Sur, and U. Ünlüata, Modeling of hydraulically controlled exchange flow in the Bosphorus Strait, *J. Phys. Oceanogr.*, *20*, 945–965, 1990.

Özsoy, E., and U. Ünlüata, Ocenography of the Black Sea: A review of some recent results, *Earth Sci. Rev.*, *42*, 231–272, 1997.

Pratt, L., Hydraulic control of sill flow with bottom friction, *J. Phys. Oceanogr.*, *16*, 1970–1980, 1986.

Pratt, L., H. Deese, S. Murray, and W. Johns, Continuous dynamical modes in straits having arbitrary cross sections, with applications to the Bab al Mandab, *J. Phys. Oceanogr.*, *30*, 2515–2534, 2000.

Seim, H., Acoustic backscatter from salinity microstructure, *J. Atmos. Oceanic Technol.*, *16*, 1491–1498, 1999.

Seim, H. E., and M. C. Gregg, Detailed observations of a naturally occurring shear instability, *J. Geophys. Res.*, *99*, 10,049–10,073, 1994.

Seim, H. E., and M. C. Gregg, The importance of aspiration and channel curvature in producing strong vertical mixing over a sill, *J. Geophys. Res.*, *102*, 3451–3472, 1997.

Seim, H. E., M. C. Gregg, and R. Miyamoto, Acoustic backscatter from turbulent microstructure, *J. Atmos. Oceanic. Technol.*, *12*, 367–380, 1995.

Signell, R., and W. Geyer, Transient eddy formation around headlands, *J. Geophys. Res.*, *96*, 2561–2575, 1991.

Tolstoy, L., *War and Peace*, Konemann, Cologne, Germany, 2000.

Ünlüata, U., D. G. Aubrey, Z. Belberov, V. Eremeev, and M. Vinogradov, International program investigates the Black Sea, *Eos Trans. AGU*, *74*, 401–412, 1993.

Winters, K. B., and H. E. Seim, The role of dissipation and mixing in exchange flow through a contracting channel, *J. Fluid Mech.*, *407*, 265–290, 2000.

M. C. Gregg, Applied Physics Laboratory, University of Washington, 1013 NE 40th St., Seattle, WA 98105-6698, USA. (gregg@apl.washington.edu)

Emin Özsoy, Institute of Marine Sciences, Middle East Technical University, P.O. Box 28, Erdemli, Içel 33731, Turkey.